Enhancing the Ti-PEKK hybrid joint by changing the PEKK crystal morphology

Master Thesis

F.F. Visser
s1742722

Faculty of Engineering Technology
Department of Mechanics of Solids, Surfaces & Systems (MS3)
Surface Technology and Tribology (STT)

Examination committee:
prof. dr. ir. M.B. de Rooij
dr. J. Seyyed Monfared Zanjani
dr. M.I. Abdul Rasheed

Document number:
ET-MS3-STT 22-2381
27th of September 2022

UNIVERSITY OF TWENTE.

ABSTRACT

The weight of an aircraft determines its fuel consumption and emissions. Therefore, the aviation industry is constantly looking for lightweight and durable material alternatives. Composite structures in general and thermoplastic composites, in particular, are finding increased use in the next generation of aircraft. However, the successful adaptation of thermoplastic composites into the superstructure depends on the development of reliable joining methods. Co-consolidation is developed as an attractive method where a metal and composite part are joined during the consolidation step.

In the current hybrid thermoplastic composite joint between CF/PEKK and Titanium, a thin interlayer of PEKK material is used to allow full wetting of the interfaces. This interlayer was shown to be a limiting factor in increasing the overall joint strength. To produce a tougher joint it is necessary to increase the toughness of the PEKK interlayer. Research has shown that changing PEKK crystal structure by decreasing the spherulite size can be beneficial for the toughness.

Herein, GNP is used as a nucleation agent for the PEKK polymer, decreasing the spherulite size by creating a dense nucleation field. Through the use of only 0.01 wt% GNP in the polymer the typical diameter for nucleation is shrunk from 46 µm to 9 µm. However, the nucleation density of the material was not homogeneous. To accurately characterise the inhomogeneities in the nucleation field a wider view of crystal distributions is combined with image recognition to create a numerical map of the nucleation field. Each map contains more than one million nuclei for the nucleated samples. Areas of low and high nucleation density were present, creating an inhomogenity in the material. The cause was determined as the polymer particle size which is a limiting factor in the mixing procedure of PEKK and GNP. To decrease the inhomogeneities of the the as received polymer was seived to a small aggregate size, below < 140 µm. Using this sieved grade of material created an on average denser nucleation field due to the disappearance of the low-density areas. These results were confirmed by the thermal characterisation of the nucleation process in DSC testing.

An alternative mixing method was also utilised, powders were pressed out to a film, such that the polymer and GNP can mix under melt conditions. This method is found to work and created even better results than through the use of the sieved polymer and is recommended for further research.

Second, the polymer materials with the altered crystalline structure are mechanically tested to evaluate the mechanical performance of the PEKK material with a small crystal size. In tensile testing, the performance of the PEKK/GNP polymers with the inhomogeneous crystal structure showed very poor mechanical performance. Most of these samples showed brittle failures. The samples produced from the sieved polymer with GNP showed much better performance but did not outperform the pure PEKK samples.

Contents

GLOSSARY

List of abbreviations

PEKK	poly-ether-ketone-ketone
PEEK	poly-ether-ether-ketone
PAEK	poly-aryl-ether-ketone
GNP	graphene nano platelet
CFRP	Carbon fibre reinforced polymer
DMF	Dimethylformamide
NMP	N-Methyl-2-pyrrolidone
GBL	γ-butyrolactone
IPA	Isopropyl alcohol
DSC	Differential scanning calorimetry
HSM	Hot stage microscopy
DCB	Double cantilever beam
SEM	Scanning electron microscopy
XPS	X-ray photoelectron spectroscopy
TEM	Transmission electron microscopy
DIC	Digital image correlation

List of symbols

ΔG	Gibbs free energy	J
ΔG_c	free enthalpy of a crystal	J
r	crystal radius	m
γ	interfacial energy	$\mathrm{mJ\,m^{-2}}$
T_m	melting point	°C
T_c	peak crystallisation temperature	°C
T_g	glass transition point	°C
ρ	density	$\mathrm{g\,cm^{-3}}$
E	Youngs' modulus	GPa
σ_y	Yield strength	MPa
ϵ_y	Strain at yield	%
$N0$	nucleation density	$\mu\mathrm{m^{-2}}$
ΔH	Enthalpy of fusion	$\mathrm{J\,g^{-1}}$
x_c	relative crystallinity	%
d	Distance available for crystal growth	µm

1 INTRODUCTION

The search for lightweight methods to attach materials while retaining high stiffness and durability is a general challenge and has existed for many centuries. But since the inception of flight, this art has become more critical, penalties for weight and failure were far greater than before. Heavier planes require more fuel for the same payload compared to a lighter planes. As a compounding detriment additional lift needs to be generated for the extra fuel. According to BloombergNEF every day 4.5 million barrels of jet fuel are used in aviation [6] contributing the global carbon dioxide emissions with 2.5 % [27]. Due to the scale even marginal improvements in the efficiency of aircraft can therefore have a measurable impact on the utilisation of hydrocarbon fuels and CO_2 and NO_x emissions. Emissions from aviation are still on the rise, which is wholly due to global demand increasing, growing from 1.89 trillion km flown in 1990 to 8.26 trillion km in 2018. Efficiency increases in aviation have largely damped the effect of this rise. Reducing the CO_2 intensity in aviation from $1\,kg\,CO_2$ per passenger kilometre in the 1960's to 0.102 kg in 2013 and further down to 0.090 kg in 2019 [26, 27]. To further these gains intensive research and development are conducted on decreasing drag, increasing engine efficiency and decreasing structural weight.

Within aircraft structures and production systems performance typically is the ratio between the strength of the structure relative to its weight. The capabilities of the materials used, together with the geometry determine this performance on a part level. However, when designing an aircraft integrating the sum of its parts is perhaps the most challenging process. These joining interfaces that emerge are ripe for significant improvements.

Joining parts can be accomplished through a plethora of methods but only some are suitable for the high demands of aerospace applications. Historically in the aerospace industry rivets and bolts were used to fasten aluminium or steel plates. The hum ble rivet was used extensively in aircraft construction. Visually the use of rivets is distinctly recognisable from the dotted grids seen on many aircraft. Over the years many developments were made to these fastening methods for enhanced strength, reliability and also aerodynamic gains. Such as the introduction of flush rivets for improved aerodynamics by removing surface protrusions. Also the move to lighter weight titanium rivets for the development of the state art blackbird aircraft programs [37]. With these improvements, rivets still create stress concentrations and cannot utilise the entire overlapping area of the materials as the rivets need to be spaced out [45].
Bonding with the use of adhesives can allow for stronger and stiffer joints. Adhesives in aerospace have been taking off since the first applications in glueing metal panels in the Fokker F27 Friendship [4]. Developing these early adhesives led to many different new thermosetting adhesives with the category of epoxies being the real workhorse. Next to the joining methods the materials used have also changed. Half of the structural mass of modern aircraft such as the Boeing 787 and the Airbus A350 is comprised of carbon fibre-epoxy composite material [38]. Joining using these curing adhesives works well with these composites as they themselves are also part epoxy. A wide range of structural parts are made of composites as can be seen in figure 1.1.

The use of thermosetting adhesives and structural components is not very sustainable with the current technologies as a circular recycling path is not possible [39, 42]. Currently, the development of thermoplastic composites is gaining traction. Thermoplastic composites in general have pronounced advantages over their thermosetting counterparts. Showing higher impact resistance, toughness and the possibility to melt process these materials have the potential to reduce production costs [31]. But most important due to the possibility to remelt the material reforming and true recycling is possible.

Due to the low reactivity of typical high performance thermoplastic materials, bonding is an active research field. Advances have been made in bonding titanium components to thermo-

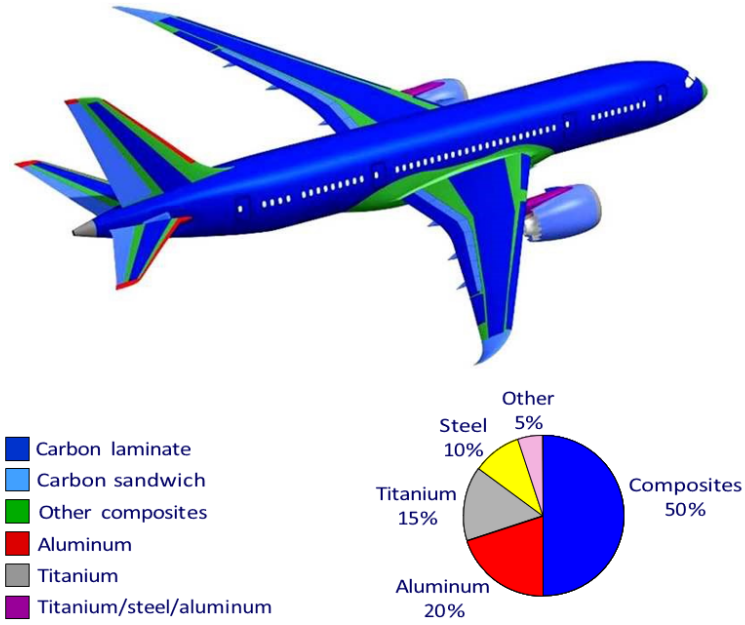

Figure 1.1: Composites use in the Boeing 787 [44]

plastic composites through the application of an extra film to effectively wet the surfaces. This bond relies almost fully on mechanical interlocking for attaining its strength [52, 33, 34] and currently fails in the pure PEKK interlayer. To strengthen this thin area graphene nano platelets are employed to try to change the local crystal morphology with the goal of improving the toughness of this critical interlayer.

2 THEORETICAL BACKGROUND

To introduce the reader to the concepts discussed in this thesis some necessary knowledge is presented in this chapter. Beginning with the introduction of polymers and their crystallinity followed by the mechanics and kinetics of the crystallisation process.

2.1 Polymers

Since the accidental discovery of polyethylene in 1898 [3], polymer science has been searching for better polymers and improving upon existing polymers. A sought-after combination is a polymer with a high temperature for its transition to the rubbery state (Tg) such that it allows use at elevated temperatures, high toughness and stiffness, combined with an acceptable melting point. These polymeric materials consist of long chain like molecules. Compared to other materials they have extreme molecular weights ranging from 10^4 to 10^6 g/mol which is orders of magnitude higher than ordinary materials such as glucose with 180 g/mol or 17 g/mol for ammonia. When many of these chains are clumped together we call the macro scale material a plastic. The molecular chains of the polymer are held together by covalent bonds which are strong attractions. Many aspects of these chains on the molecular scale determine the eventual macroscopic properties. One of great importance is the structure or lack thereof. A bulk of completely unordered polymer chains are called an amorphous state, directly taken from the Greek meaning "*without shape*". In such cases, the polymer chains are tangled and unordered like a plate of cooked spaghetti.

2.2 Polymer crystallinity

In many polymers, the amorphous or randomly oriented state is not the state that is most energetically favourable. During cooling parts of these long molecules can align and fold to create regular patterns within the bulk. Whenever the temperature of a polymer is below the melting point, then the free enthalpy of a crystal formation will be lower than that of the amorphous state. This difference in energy drives the formation of crystals.

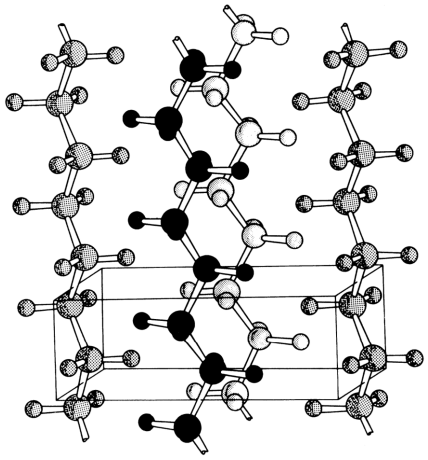

Figure 2.1: Crystal structure of polyethylene (chains coloured differently for clarity) [9]

2.2.1 Homogeneous nucleation

Crystallisation occurs in two distinct stages. First, a nucleus needs to be formed, from which the crystal can grow. Nuclei formation occurs in pure polymers through homogeneous nucleation. Forming a stable nucleus is a stochastic process driven by random motion of the polymer chains. The energies involved however are not random. Below T_m the difference in free enthalpy of the crystal (ΔG_c) is driving the formation, but a crystal has a different structure and thus forms an interface with the rest of the amorphous bulk. For a nucleus ΔG_c scales with the volume of the nucleus and the interfacial energy (γ) with the area. The potential between these two states is then:

$$\Delta G = -\frac{4}{3}\pi r^3 \Delta G_c + 4\pi r^2 \gamma \tag{2.1}$$

Below a critical radius, the interfacial energy is too high to sustain the crystal and it dissolves again in the bulk. Beyond the critical radius, the nuclei is stable and can grow. The way these chains can 'fit' together depends mostly on the molecular structure. For example a highly linear polymer such as polyethylene can align fairly easily due to its regular and straight molecular structure. In figure 2.1 this structure can be seen. In a polymer bulk the material is still an entangled cluster of long chains. Therefore chains cannot naturally fully crystallise and form one macro scale crystal such as in some minerals or special metals. For that scale of untangling to occur is entropically impossible. Only in smaller local sections the chains can align to find the energetically lower configuration. Polymers that exhibit these areas of local crystallinity are called semi-crystalline polymers.

2.2.2 Heterogeneous nucleation

The boundary between two materials always presents a situation with more interaction and possibility than the depths of a bulk material. In a polymeric bulk the chains act upon each other but move and reptate randomly depending on the temperature. By adding a foreign material this movement can be constrained or guided. On the Interface between polymer and foreign materials a transcrystalline region can be found in specific combinations of materials. If the foreign material can nucleate the polymer crystallization in large numbers, the growing crystals impinge and are constrained in the direction parallel to the interface. Therefore crystal growth presents itself in the direction perpendicular to the interface. For a transcrystal the nucleation density is high resulting in neighbouring crystal impinging and forming nearly perpendicular growth from the interface. In literature the foreign material tends to nucleate under the following conditions [13]:

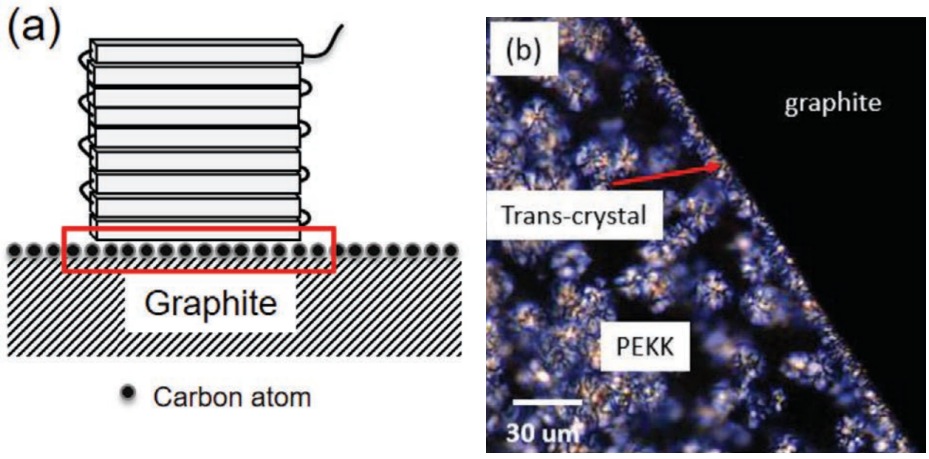

(a) Representation of a flat-on PEKK crystal on a graphene interface [17]

(b) Formation of a transcrystalline structure on a PEKK - graphene interface [17]

- Geometrical match
- Difference in thermal conductivity
- Polymer alignment due to extensional flow
- High surface free energy of foreign material

Research at the UNIVERSITY OF TWENTE found in 2020 that graphene can create a dense area of transcrystal in the poly-ether-ketone-ketone (PEKK) polymer [17]. It was found that against

graphite the PEKK polymer chains form a cyrstal lamella where the polymer direction is parallel with the graphite surface [16].

The molecular geometry of PEKK and graphene seem to match. The aryl group is similar in structure to the hexagonal lattice present in graphene. The hexagonal lattice of graphene has a bond length of 0.142 nm, where the C-C bond in PEKK has a length of 0.154 nm and the double bonded carbon has a length of 0.134 nm. The two materials also have vastly different thermal conductivities. PEKK has been tested to have a thermal conductivity of 0.178 W/mK which falls within the typical values for thermo plastic composites. Graphene is reported to have a thermal conductivity of around 3000 W/mK [36]. Distancing the values of the two materials by nearly four orders of magnitude.

2.2.3 Crystal growth

With the formation of a stable nucleus either through homo- or heterogeneous nucleation the local crystal can grow outward. In the absence of a temperature gradient the crystal grows from the nucleus orientation, forming the first lamellae. Aside from the existing lamellae, new growing lamellae with slight differences in orientation can be nucleated on the growth front. In continued growth these small misalignments add up forming a radially expanding growth front as can be seen in figure 2.3.

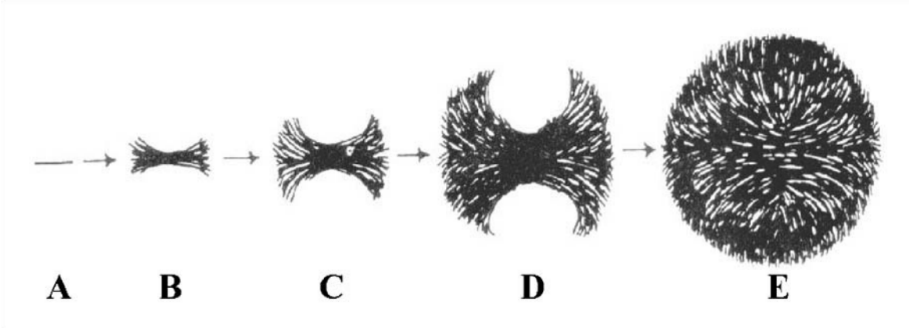

Figure 2.3: Schematic growth of spherulites from lamella [25]

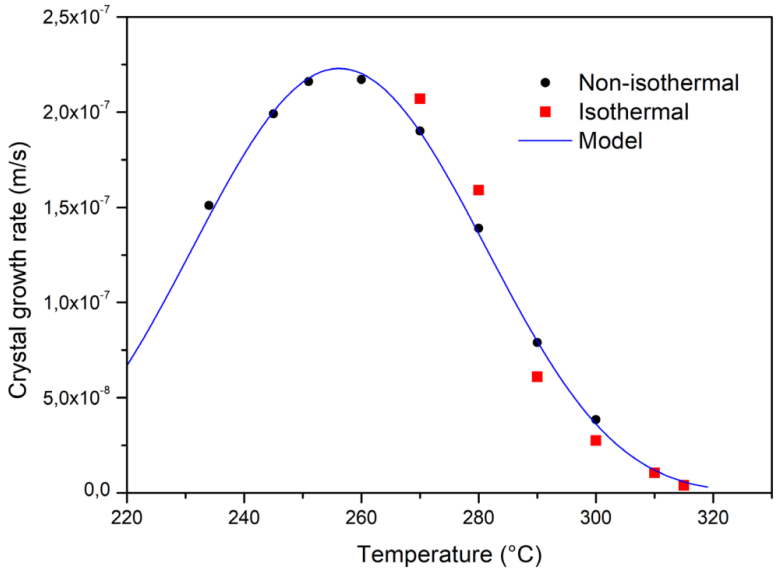

Figure 2.4: Experimental growth rate found for PEKK 70/30 as a function of the isothermal crystallisation temperature. The black dots and red squares are from experimental data and the solid blue line refers to the Lauritzen-Hoffman model that was identified on the data [11].

Growth of the crystal is still driven by ΔG_c which is a function of the degree of supercooling. The movement of the polymer chains is inversely related to the temperature. At lower temperatures viscosity and the chain length hinder the movement of the polymeric bulk until T_g below which where no relative chain movement is present. These two counteracting effects create a bell-shaped curve for the crystal growth rate. By tracking the growth of individual spherulites using a polarised hotstage microscopy (HSM) setup for PEKK with a (T/I) ratio of 70/30 Chelaghma et al. found that the temperature of peak growth is 255 °C with a growth rate of $2.2 * 10^{-7}$ m/s. This growth rate is valid for both isothermal and non-isothermal as the rate is only dependent on the temperature and is independent of the cooling rate. The full curve is presented in figure 2.4

2.3 Poly aryl polymers

The category of fully aromatic polyetherketones was first reported by Bonner in 1959 [8], however in a low molecular weight. The process for producing higher molecular weight polyaryletherketones (PAEK) using diaryl sulphones for the condensation reaction was published by Attwood et al [2]. In these studies, it was already noticed that increasing the ketone content of the polymer increases the Tg but has a larger effect on the melting point. From this family of polymers poly ether ether ketone (PEEK) first found commercial success. In the dental industry PEEK was found to be a useful alternative for titanium, due to its mechanical properties such as high strength, biocompatibility, negligible water absorption and heat resistance [47].

In further developments, PEKK was made boasting even higher stiffness than PEEK [10]. For further commercial application the production process was improved and commercialised by DuPont. In this process the polymer is synthesised from three precursors. In production, these are diphenyl ether (DPE), terephthalic acid (T) and isophthalic acid (I). Poly-Ether-Ketone-Ketone is defined as having one-part ether bonds and two-parts ketone bonds between the aryl groups, as indicated by the name. This ratio is created by reacting one part DPE with

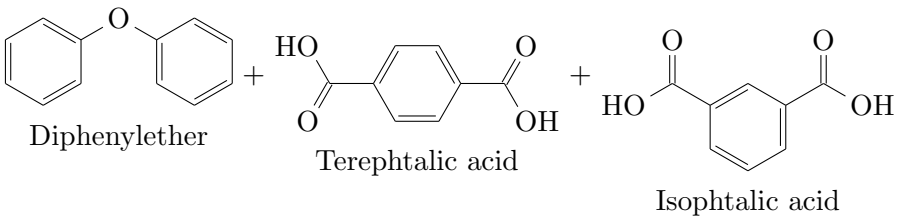

Figure 2.5: precursors used for synthesising PEKK [23]

two parts T or I. T and I differ in one important property, the spacing of the acid groups around the benzene group is not the same, as can be seen in figure 2.5. Terephtalic acid has the acids on opposite sides of the benzene creating a straight connection, called a para linkage. Isophtalic acid has the acid groups spaced two links apart, creating an angle in the molecule, called a meta link. In figure 2.6 a section of the PEKK chain is presented that contains two repeat units, the left showing a para linkage resulting from the T precursor and the right section was made from I and at the very end shows a meta linkage. Such an irregularity in the polymer chain hinders the alignment of the chains. Therefore the crystal structure cannot be as regular which influences the melting point, the typical undisturbed crystal repeat unit can be seen in figure 2.7. For industry incorporating the meta to para links in the polymer allows the melting point to be lowered by changing the crystal alignment [23], which is in the interest of processability.

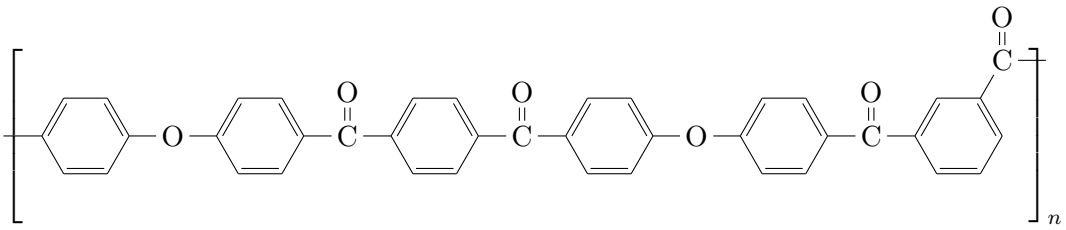

Figure 2.6: Two poly-ether-ketone-ketone monomer repeat units, the first being made from T and the second from I [23]

For example, in the extreme case of a PEKK grade made with a (100/0) T/I ratio the polymer is very stable at high temperatures, pushing its melting point beyond the thermal degradation point and therefore making it unusable in practise [23]. Thus the combination of para and meta linked ketone groups allows the melting point of the macro material to be tuned.

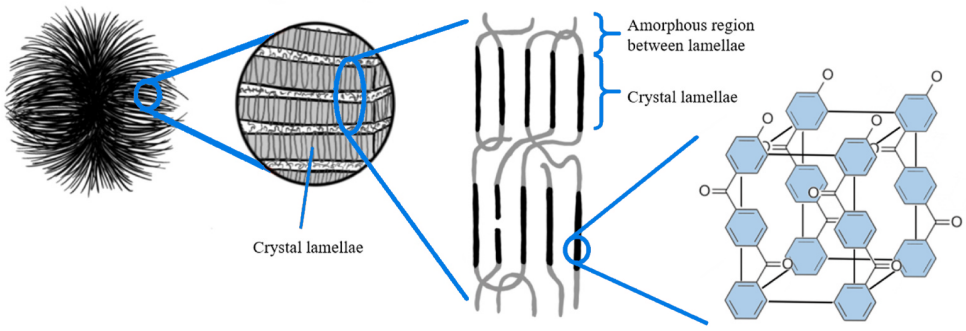

Figure 2.7: Crystal structure in polyaryl polymers [41]

2.4 Thermoplastic composite joints

In the interest of sustainability and higher strength materials, thermoplastic composites are gaining more use in industry. To incorporate these parts in a larger structure they need to be integrated either through a bonding method. For thermoplastic composites the matrix material is used to bond the fibres together to attain the strength of the macro material. This bonding mechanism has been investigated for bonding to different materials other than carbon fibers. In aerospace, a bond with titanium is of interest to incorporate threaded parts in a composite structure while still retaining a low weight. The unique possibility that arises with thermoplastic materials is the processing of a hybrid joint during the consolidation steps. Research to investigate this possibility is presented hereafter.

2.4.1 Co-consolidation of Titanium-C/PAEK Joints

Within the UNIVERSITY OF TWENTE research effort has been put into the understanding and development of co-moulding setups for more than a decade. As more research effort was put into thermoplastic composites as opposed to thermosets related techniques in processing and fastening changed as well. Within the University this avenue of research was started by Yibo Su [51]. In his dissertation, an initial investigation in to the interfacial performance of co-consolidated Titanium-C/PAEK joints was performed. The focus was laid on dissecting the contributions of different adhesion mechanisms. The three mechanisms of adhesion that were investigated were Mechanical interlocking, chemical bonding and physical adhesion. A fourth aspect of the bond performance is the presence of residual thermal stresses. The major contributor to the interfacial performance was identified as mechanical interlocking as increasing the surface roughness had a tremendous effect on the bond performance. Titanium surfaces were roughened by grit blasting them with various media, with aluminium oxide showing the best results. Furthermore, it was determined with a theoretical model that a larger degree of roughness could benefit the bond strength even further. Chemical bonding is possible to occur between PEKK and Titanium by forming a connection between the Titanium and the double-bonded oxygen of the ketone group [20]. By X-ray photoelectron spectroscopy (XPS) the presence of these bonds was confirmed on fractured mandrel peel specimens, therefore confirming the presence of chemical bonding. The effect of chemical bonding is dependent on mechanical interlocking for the bond performance as this effect is only present on an atomic scale. In Ti-C/PEKK bonded specimens the Physical attraction was judged to contribute but on a nearly negligible scale compared to the other two effects. This was determined by comparing the fracture energy from mandrel peel testing to the calculated work of adhesion developed from contact angle measurements, as there was little correlation this effect is small and not very relevant.

2.4.2 Effect of grit-blasting on the fracture toughness of hybrid titanium-thermoplastic composite joints

Continuing the research line on the co-consolidated titanium-C/PAEK joint Vanessa Marinosci performed primarily experimental research instigated by the findings of Yibo Su. As mechanical interlocking is a major contributor to the bond strength the optimal roughness for the titanium surface was yet to be determined. Thus the research avenue Vanessa Marinosci investigated was the influence of the titanium surface roughness on the interfacial strength experimentally [33]. Through extensive mandrel peel testing with titanium substrates and unidirectional C/PEKK. The titanium surface roughness was changed by changing the grit blasting pressure. With only

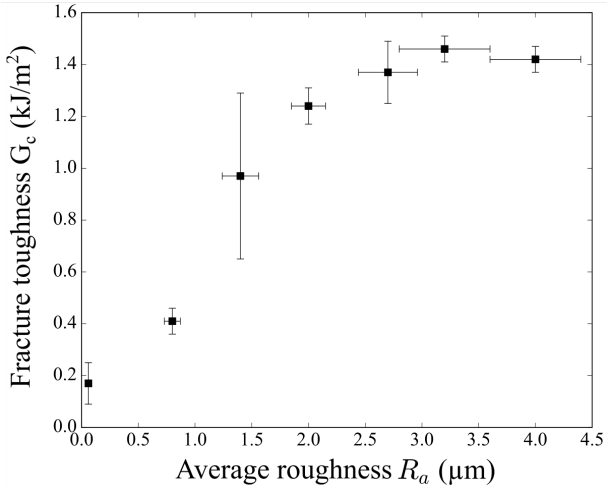

Figure 2.8: Fracture toughness results with respect to the average roughness of the different titanium surfaces. [33]

the pressure as the variable the created surfaces have an autocorrelation length implying that the surface topography is similar. Increasing the pressure creates deeper asperities resulting in a higher mean arithmetic roughness known as Ra. The results can be seen in figure 2.8. An increase in roughness resulted in a higher fracture toughness until a plateau that starts at a roughness of Ra 2.5 μm, corresponding to a blasting pressure of 3 bar. Further increasing the blasting pressure and thus the roughness did not result in further large improvements of the fracture toughness. At higher roughnesses the cohesive failure happening in the Titanium-PEKK interface tends to move into the composite material. Thereby moving the failure from the interface between the metal and the composite to the interface between the matrix material and the fibres.
In the titanium hybrid joint the polymer interlayer between the thermoplastic composite and the titanium proved to be the weaker link causing a local failure that formed a crack. Such a crack can grow and move in to the composite material to cause intra-ply failure. To prevent such cases it is a interest to toughen this interlayer to attain an overall stronger bond. Initial testing for improving the interlayer toughness is shown below.

2.4.3 Improving the Ti/PEKK joint performance by tuning the interphase crystalline structure using graphite nano-plates

In a bonding interface ductility is of great importance and is captured typically in fracture energy values. In polymer science it is postulated that a PEKK polymer with a smaller crystal morphology can deform more before failure. Typically a smaller crystal morphology would be attained by changing the thermal processing of the polymer. However aerospace parts are

generally made in an autoclave that can realise slow cooling and heating rates. Thus to get a smaller crystal size Doddahanumegowda tried to nucleate the PEKK polymer using graphene nano platelets (GNP) to get the same effect while remaining compatible with an autoclave process [19].

GNP was dispersed through the PEKK polymer in a cold process by mixing in a acetone bath

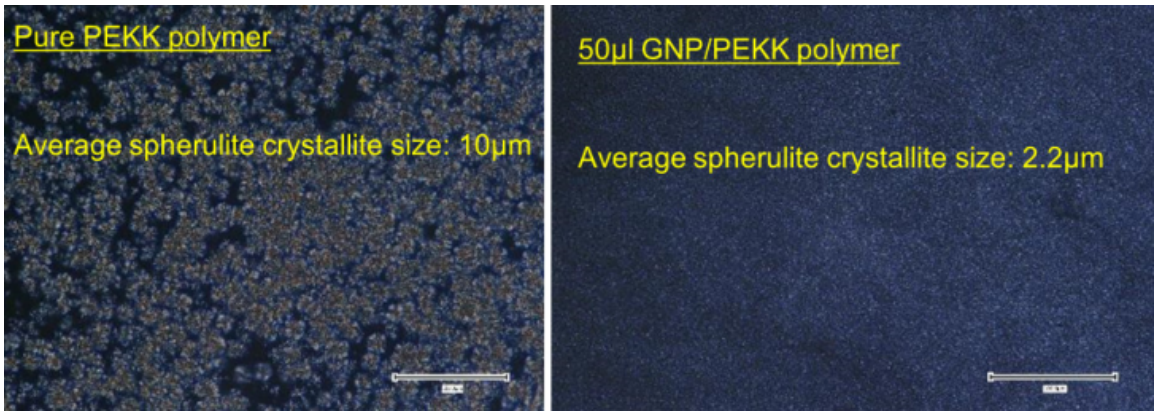

Figure 2.9: HSM image of PEKK and PEKK with 0.05 wt% GNP [19]

and dispersed by ultra sonication. The acetone was then evaporated which left a dry powder. Doddahanumegowda produced two different concentrations of the PEKK-GNP dispersion, 0.01 wt% and 0.05 wt%. To test the effect of adding GNP to the polymer it was mechanically tested by a double cantilever beam (DCB) test in a sandwich between two titanium strips. The samples that were made with GNP in the PEKK adhesive show a higher fracture toughness of 2.4 kJ/m^2 compared to 1.7 kJ/m^2 for the specimens without GNP. Thus lacing the PEKK with GNP shows promise to improve the fracture toughness in the bond.

In this research several challenges were identified. First, the quality of the mixture of the GNP through the PEKK granules was suboptimal. One snapshot of the HSM images is presented in figure 2.10 In the HSM images many areas contained streaks with very high nucleation density indicating clusters of GNP while other areas had very low nucleation density. This inhomogeneity of the material is not optimal. Second the extension to the carbon fibre reinforced polymer (CFRP)-PEKK interface is unknown as only the TI-PEKK interface was tested.

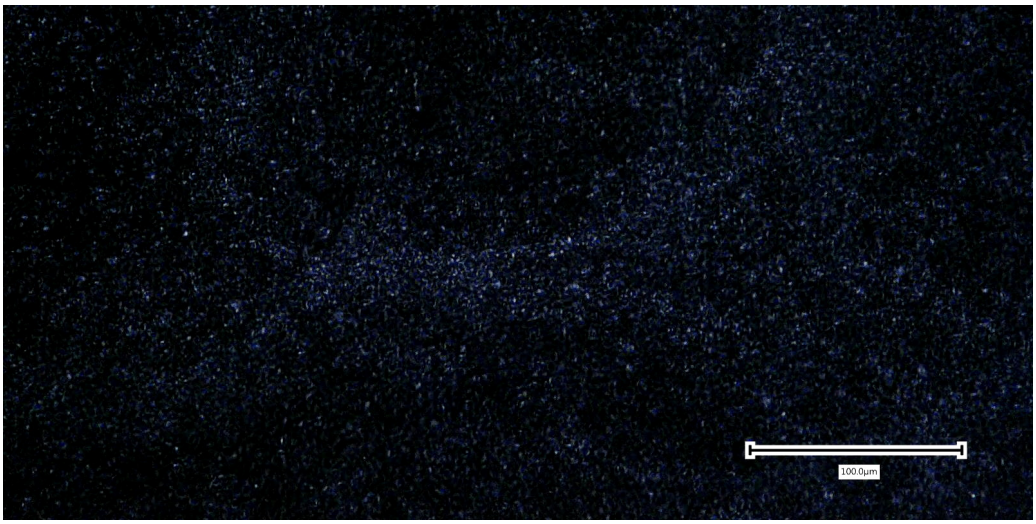

Figure 2.10: HSM image showing streaks of high nucleation density in PEKK with 0.01 wt% GNP at 316 °C during cooling at 4 °C/min [19]

2.5 Graphene addition to poly aryl polymers in literature

In composite manufacturing, a strong fibre is combined with a more ductile matrix material to form a strong macro material. For the fibre material in a matrix, a host of materials is used but mainly glass fibres or carbon fibres are used. However the use of nano fillers is on the rise, nano fillers allow the modification of bulk material with only little additive percentages. These nano filler materials are isolated to a molecular level.
In the case of graphene nano flakes the material is purely a two-dimensional hexagonal lattice of carbon atoms. The sizing of graphene flakes varies between suppliers and grades but typically a flake has a lateral size between 30 and 180 μm and a thickness of about three layers up to 30 layers depending on the quality of exfoliation [57, 58, 43]. Graphene has multiple excellent properties that make it interesting as a filler material. First the thermal conductivity is ten times higher than copper, has outstanding electrical conductivity and has an in-plane stiffness of 1060 GPa [50] at a cost price that is not a large deterrent. Therefore the addition of this material to polymers could in theory counteract the electrically and thermally insulating properties of polymers or improve mechanical properties.
So far in research graphene has been added to polymers mainly to improve their electrical conductivity [56] for applications in electronics or for enabling technologies such as induction welding. In other cases, the goal is to improve the thermal conductivity of the material to ease processing conditions such as 3D print applications [12]. As PEKK is a high-performing but also expensive and currently quite niche material the body of research is limited. In commercial applications PEEK is the polyaryl polymer that sees the most use in industrial applications. For this closely related polymer much more research has been conducted, also on the specific topic of adding graphene to improve mechanical properties. Therefore studies that for various reasons reported on tensile testing results of PEEK with graphene mixed in are discussed hereafter.
In these studies, various GNP filler concentrations are used, up to 10 wt%. Results show that graphene can improve the young's modulus of the materials by up to 40%. Which is reported as the singular upside for the mechanical properties of the polymer. The ductility of the material shows a sharp decline after a certain concentration of GNP. The lowest filler concentration that decreased the ductility was 0.2 wt% in the research of Xu [59], 0.5- 1 wt% for Chen [12], 1 wt% for Puertolas and 2 wt% for Wang [56]. The full mechanical testing results including their mixing method from the literature are summarised in table 2.1. Above a certain GNP concentration the consensus is that the clumps of graphene have low resistance to shear. If these areas start to fail first they act like stress raisers and will even form voids locally. Therefore if ductility is required increasing the graphene content above 1 wt% is not productive.

Table 2.1: Tensile testing of polyaryl polymers with added graphene in literature

polymer	supplier	GNP mixing method	supplier	flake size up to [μm]	concentration %wt	Tensile test shape	testspeed [mm/min]	Young's [Gpa]	Tensile [Mpa]	Strain at break [%]	study
PEEK	Changchun Uni	solvent (diphenyl sulfone)	Strem Chemical:	50	-	-	-	1.99	96.20	19.17	[59]
py-PAEK	Changchun Uni	solvent (diphenyl sulfone)	GNP	50	0.2	-	-	1.87	98.43	31.59	[59]
py-PAEK	Changchun Uni	solvent (diphenyl sulfone)	f-GNP	50	0.2	-	-	1.95	98.52	63.17	[59]
py-PAEK	Changchun Uni	solvent (diphenyl sulfone)	GNP	50	0.5	-	-	2.07	100.40	16.84	[59]
py-PAEK	Changchun Uni	solvent (diphenyl sulfone)	f-GNP	50	0.5	-	-	2.16	105.48	54.89	[59]
py-PAEK	Changchun Uni	solvent (diphenyl sulfone)	GNP	50	1	-	-	2.05	95.74	15.73	[59]
py-PAEK	Changchun Uni	solvent (diphenyl sulfone)	f-GNP	50	1	-	-	2.06	101.14	42.67	[59]
PEEK	Victrex 150P	EOS electric powder mixer	2-DTech	26.5	0	film 250 μm	20		82.60	5.03	[12]
PEEK	Victrex 150P	EOS electric powder mixer	2-DTech	26.5	0.1	film 250 μm	20		103.10	6.65	[12]
PEEK	Victrex 150P	EOS electric powder mixer	2-DTech	26.5	0.5	film 250 μm	20		100.00	6.12	[12]
PEEK	Victrex 150P	EOS electric powder mixer	2-DTech	26.5	1	film 250 μm	20		90.42	5.05	[12]
PEEK	Victrex 150P	EOS electric powder mixer	2-DTech	26.5	5	film 250 μm	20		60.00	2.36	[12]
PEEK	Victrex 150P	EOS electric powder mixer	2-DTech	26.5	10	film 250 μm	20		55.77	2.06	[12]
PEEK	Victrex 150P	sonicated in ethanol	2-DTech	26.5	0.1	film 250 μm	20		96.642	6.59	[12]
PEEK	Victrex 150P	sonicated in ethanol	2-DTech	26.5	0.5	film 250 μm	20		101.598	6.10	[12]
PEEK	Victrex 150P	sonicated in ethanol	2-DTech	26.5	1	film 250 μm	20		92.512	4.98	[12]
PEEK	Victrex 150P	sonicated in ethanol	2-DTech	26.5	5	film 250 μm	20		55.6	2.29	[12]
PEEK	Victrex 150P	sonicated in ethanol	2-DTech	26.5	10	film 250 μm	20		45.6	2.00	[12]
PEEK	Victrex 150P	extrusion compounding	avanPLAT-40	40	0	ISO-527:1-1AB	10	3.61 ± 0.08	105.6 ± 2.1	20.1 ± 1.5	[43]
PEEK	Victrex 150P	extrusion compounding	avanPLAT-40	40	1	ISO-527:1-1AB	10	3.71 ± 0.29	98.6 ± 5.2	8.2 ± 0.5	[43]
PEEK	Victrex 150P	extrusion compounding	avanPLAT-40	40	3	ISO-527:1-1AB	10	3.86 ± 0,44	96.5 ± 5.5	4.5 ± 0.4	[43]
PEEK	Victrex 150P	extrusion compounding	avanPLAT-40	40	5	ISO-527:1-1AB	10	3.81 ± 0.50	95.4 ± 7.2	4.4 ± 0.3	[43]
PEEK	Victrex 150P	extrusion compounding	avanPLAT-40	40	10	ISO-527:1-1AB	10	5.20 ± 0.51	88.5 ± 4.2	2.2 ± 0.3	[43]
PEKK	in-situ polymerisation	sintered		120	0	ASTM 638-V	10	2.0	220.0	15.6	[56]
PEKK	in-situ polymerisation	sintered		120	2	ASTM 638-V	10	3.1	187.0	6.2	[56]
PEKK	in-situ polymerisation	sintered		120	3	ASTM 638-V	10	2.6	116.3	4.2	[56]
PEKK	in-situ polymerisation	sintered		120	4	ASTM 638-V	10	2.9	156.0	5.2	[56]
PEKK	in-situ polymerisation	sintered		120	6	ASTM 638-V	10	2.8	177.0	6.0	[56]

2.6 Mixing methods for dispersing GNP in PEKK

For nucleation effects, only the surface area of the alien material is required for nucleating the polymer bulk. This is an interfacial phenomenon that is enabled by properties mentioned before in section 2.2.2. To maximise the graphene surface area that is available for the polymer to nucleate against it is paramount to avoid the agglomeration of the graphene flakes and thus disperse the flakes evenly throughout the polymer. This is hindered by significant Van der Waals forces that are present between platelets and drive them to clump together [49]. Many chemical methods have been evaluated in the context of exfoliating graphene from a graphitic bulk. Generally in these top-down production methods for exfoliation to GNP a combination of ultrasonication and strong polar aprotic solvents are used [53]. These methods involve the combination of strong solvents such as Dimethylformamide (DMF), N-Methyl-2-pyrrolidone (NMP) or γ-butyrolactone (GBL) combined with probe or bath ultrasonication [28]. These methods are also relevant for preventing agglomeration. Flakes that have already been exfoliated are much less clustered than a pure graphitic bulk and thus milder processes can be utilised than for exfoliation. In this research the advantage is that the percentage of graphene filler used is very low compared to bulk exfoliation or production of nano composites as only a nucleation effect is desired. Concentrations for these process are in the order of 0.01 - 5 mg/ml Graphene [53]. In the context of altering the nucleation density of the polymeric bulk, it has been shown by Doddahanumegowda et al. that concentrations of up to 0.05 wt% of GNP to PEKK. In processing GNP to solvent ratio of 0.05 mg/ml at maximum. Since the concentration of GNP that needs to be stabilised is at least two orders of magnitude more dispersed than has been shown possible also less strong solvents are required and have been confirmed in research [48, 55, 58]. For retaining separation between graphene flakes acetone bath ultrasonication has been applied successfully in multiple cases [21, 48]. In mixing with polymers this process was mainly applied in processing for the creation of a blended epoxy.
An important aspect of thermoplastic polymers and especially the polyaryl family is their high melting point, typically in the range of 300 to 370 °C [1, 23, 2]. In their application, this is an advantage but in processing, it is a distinct disadvantage. In the testing performed by Doddahanumegowda et al. distinct areas of low nucleation density were identified. A likely culprit was found in the grain size of the PEKK polymer. Mixing was performed far below the melting point of PEKK. In mixing with the GNP stabilised in acetone GNP cannot penetrate into the bulk of the polymer grains. Thus the GNP can only be coated on the outside of the PEKK granules, therefore aggregate size is a limiting factor on the mixing result. The size effect of the PEKK granules is illustrated in figure 2.11. A commercial mixture of PEKK 7002 granules from Arkema typically includes sizes up to 2 mm meaning the GNP cannot be mixed directly into areas up to 2 mm, which in the context of spherulites is very large. Therefore these larger grains pose a problem in creating a homogeneous mixture since under cold conditions GNP cannot be dispersed into the polymer grains but can only coat them.

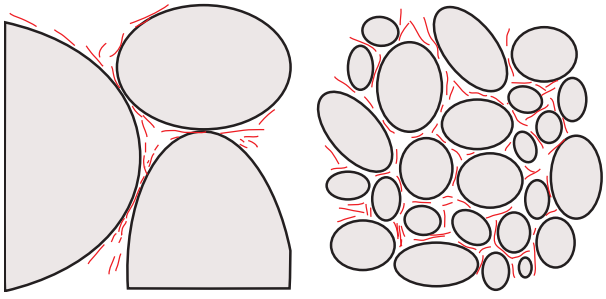

Figure 2.11: GNP dispersed within large particles (left) and small particles (right) $T << T_m$

2.7 Research goals

In aeronautical and automotive applications the role of fibre-reinforced thermoplastic composites is becoming increasingly important. It has been shown that it is possible to improve the toughness of a PEKK layer by changing the crystal morphology. However, it is as of yet not quite understood why there is a dramatic difference in the potential to absorb plastic deformation energy. The goal of the research is to attain a better understanding of the effect of changing the crystal structure of PEKK in the interfacial layer.
First, the crystal morphology that is created by adding GNP to the polymer blend will be evaluated using HSM. Here the crystal morphology, size and distribution will be evaluated. Second, the bulk material properties of a PEKK polymer containing GNP will be evaluated using tensile testing. By compression moulding dogbones will be made that conform to ISO standards. Lastly the entire interface will be evaluated by moulding a hybrid Ti-PEKK-CF/PEKK joint in an autoclave process. These samples will be evaluated using mandrel peel testing. This combination of experimental techniques provides a more in-depth understanding of the created interface and its mechanical properties.

2.8 Research questions

The main question to be answered in this report is: "What is the effect of changing the crystal morphology of PEKK through nucleating with GNP on the mechanical properties of PEKK?" This overarching question will be subdivided in three subquestions. Each subquestion highlights a specific piece of knowledge that will help to build an understanding of the larger problem.

1. How can the nucleation field homogeneity be evaluated and improved?
2. What is the effect of the mixing method on the PEKK crystal morphology?
3. What is the influence of the PEKK crystal size and distribution on its mechanical properties?

3 MATERIALS AND METHODS

3.1 Materials

3.1.1 Poly-ether-ketone-ketone (PEKK)

The PEKK polymer was kindly provided by Arkema. The polymer grade used is kepstan 7002. 70 indicates the T/I ratio of the polymer which is 70/30, meaning 70% of the ketone linkages are para linked and 30 % has a meta linkage. The 02 indicates the flow grade, which is the medium grade with a melt volume flow rate of 35 cm^3/10min for 5 kg at 380 °C [1]. The as received sample is illustrated in figure 3.1 with sizes of aggregates ranging between 10 μm and 4 mm.

Table 3.1: Relevant PEKK datasheet properties provided by Arkema [1]

ρ $[g/cm^3]$	T_m °C	T_g °C	E [GPa]	σ_y [MPa]	ϵ_y [%]
1.29	331	162	3.8	70-110	5.2

3.1.2 Graphene nano platelets (GNP)

Graphene nano platelets were purchased from XG sciences. The platelets are specified at 750 m^2/g by XG sciences. The typical structure of the platelets can be seen using Transmission electron microscopy (TEM) visible in figure 3.2. Particles are aggregates of sub-micron platelets and contain sections with multiple layers and small clusters. The lateral size of the particles is specified as being below 2 μm. When received dry nano platelets were dispersed in a bottle of acetone at a concentration of 1 gram of GNP per 100 ml of acetone and stored as such.

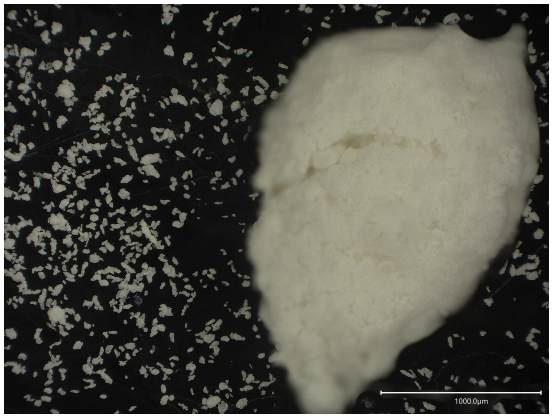

Figure 3.1: Dark field image of Kepstan 7002 indicating the scale difference between small particles and large aggregates.

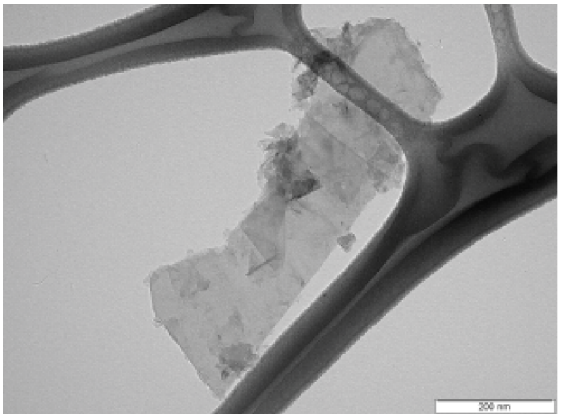

Figure 3.2: TEM image of a graphene platelet showing the clusters and aggregates of particles - 750 m^2/g [5]

3.2 Preparation methods

In the previous chapters a view of the current knowledge on PEKK crystallinity and the possible effects of adding GNP to the mix were presented. In pursuit of the answers to the research questions an experimental methodology was developed. In this chapter each step in the methodology will be thoroughly explained. To provide an overview of the total process a diagram of the material flow diagram is presented in figure 3.3.

Starting materials are indicated in green in the diagram. For the coarse particle grade the powder is used as it was received (grade C). To create a finer powder the bulk coarse powder is sieved down below a $140\mu m$ particle size (grade S). Both powders are then used in the same ultrasonic mixing procedure as is explained in detail in section 3.2. In this mixing procedure each of the two powder grades is combined with GNP either at a concentration of 0.01 wt% or 0.05 wt%. For the control powders without GNP this process is bypassed.

The microstructure of the material is analysed optically using HSM where the nucleation field can be imaged during its formation at high temperatures. Thermal kinetics of the material are evaluated using DSC, which provides insight on the crystallisation temperatures. Performance of the nano composite material is evaluated by tensile testing on compression moulded dogbone samples.

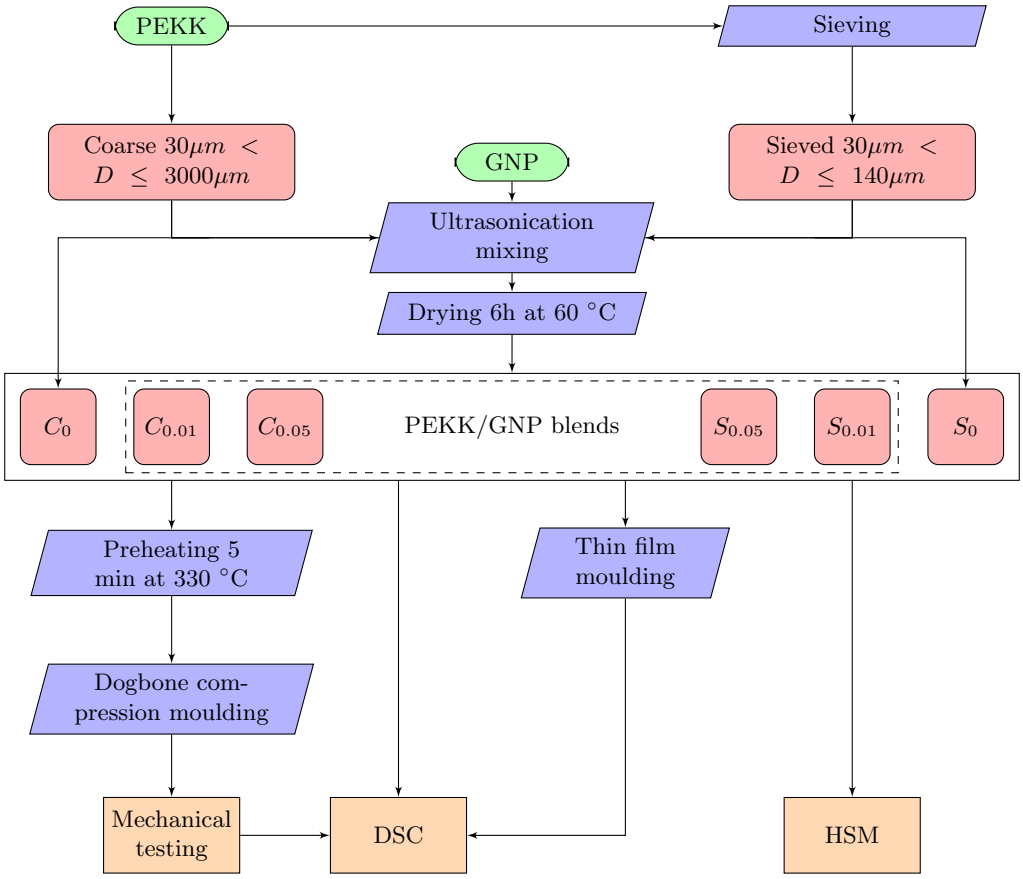

Figure 3.3: Material flow through the experimental process

To study the effect of the GNP addition on the properties of PEKK polymer samples with different dispersions of GNP were made. The first variable that is of interest for increasing the homogeneity in the polymer is the granule size. Therefore powders of two different particle sizes are used, the commercially available PEKK powder (grade C) with a wide range of particle size. Through Toray a batch of PEKK kepstan 7002 was delivered in a finely sieved powder fraction (grade S). Using optical microscopy combined with particle size recognition it was determined that the powder distribution was similar but was cut off at the 140 μm size. The second variable is the concentration of GNP in the polymer. Three variations are used; pure PEKK, 0.01 wt% and 0.05 wt% these two concentrations of GNP have been shown to provide adequate nucleation effect [19]. Together this makes for six different polymer blends that are used in the rest of the testing procedures. Properties and concentrations of these blends are presented in table 3.2.

Table 3.2: PEKK/GNP samples and concentrations used

Name	GNP solution volume [µl]	GNP weight [mg]	PEKK particle size [µm]	PEKK weigth [g]	%wt GNP
C_0	0	0	30-2000	10	0.00
$C_{0.01}$	100	1	30-2000	10	0.01
$C_{0.05}$	500	5	30-2000	10	0.05
S_0	0	0	30-140	10	0.00
$S_{0.01}$	100	1	30-140	10	0.01
$S_{0.05}$	500	5	30-140	10	0.05

3.2.1 Powder mixing procedure

As identified in earlier research and illustrated in section 2.6 the homogeneity of the PEKK and GNP mixture needs improvement [19]. Improving the dispersion of GNP through the polymer was attempted by significantly decreasing the PEKK aggregate size. The mixing procedure utilised is ultrasonic bath mixing and is performed below melt temperatures.

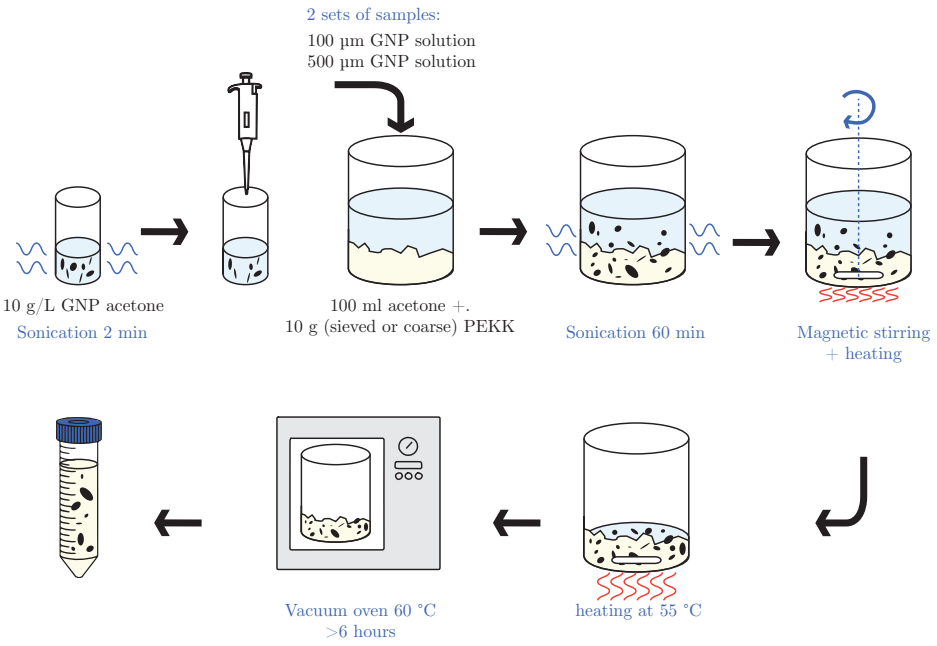

Figure 3.4: Procedure for mixing PEKK with GNP

In this process the PEKK granules are put in an acetone bath together with the GNP. This process is schematically depicted in figure 3.4. The storage bottle of acetone/GNP is sonicated for two minutes to avoid the addition of GNP agglomerates. Then, 10 grams of PEKK powder is weighed and poured in a 600 mL beaker. In 100 mL of acetone 100 µL of GNP solution is added with for the 0.01 wt% blends and 500 µL for the 0.05 wt% blends. Afterwards the beaker is placed in the SONO SWISS SW 6H ultrasonic bath with demineralised water at the same level as in the beaker. After which the mixture is sonicated for 60 minutes. The beaker is removed from the ultrasonic cleaner and a magnetic stirrer is added and then placed on the IKAMAG RCT hotplate and the temperature set to 55 °C. The stirring speed is set such that there is movement in the acetone but no turbulent mixing. Magnetic stirring is turned off when only a slurry is left, the slurry is dried off on the hotplate for 1 additional hour. The beaker is placed in a vacuum oven at 60 °C for at least 6 hours. After mixing and drying of the GNP and PEKK mixtures the dry powders are stored in sterile Greiner tubes made from polypropylene.

3.2.2 Thermal analysis preparation

After the mixing process to form the PEKK/GNP powders they were subjected to DSC testing. Three forms of polymer were to be subjected to testing: powders right after mixing, dogbones after tensile testing and pieces of the films. TA Tzero pans were used with the standard black lid (not hermetically sealed). Material was added to the pan until the scale read between 4 and 6 mg. For the dogbone samples a chunk was cut out of the middle of the top of the dogbone. Edges that had touched the mould surface or the polyimide were removed to get a sample that is representative for the bulk. Films were first cleaned with isopropyl alcohol (IPA) and then a piece was cut out near the outer edge of the samples, the outside edge itself was cut off and disposed.

3.2.3 Mechanical testing specimen preparation

Due to the possible health and safety risks that come with the use of nano materials [40] precautions were taken to ensure safe conduct for the use of large quantities, as is required with the production of tensile test specimens. In dry conditions the GNP are held in place by weak forces such as van der Waals forces and electrostatic charges, but it is possible for particles to become airborne during handling. To eliminate this risk the tubes with dry powders were only opened and used in a clean air by Baker NEG 2 cabinet. This cabinet creates a laminar airflow away from the working area after which it is immediately filtered. To allow further use of the material the GNP is embedded in the polymer by a short heating cycle. In the 125x125 mm mould a thermocouple is inserted after which it is sealed using upilex tape and placed in a preheated oven. The sample is then allowed to heat to 330 °C and kept there for 5 minutes. After this process the polymer samples are stored in air tight sample bags until further processing.

Producing tensile ISO-20753-12A specimens

Tensile testing of material unlike DSC requires a shaped specimen in order to perform the test correctly. For the production of the tensile testing samples a square mould of 125x125mm is used with a 2 mm plate insert for the shape of the specimens. With polymer processing it is paramount to avoid spillage and sticking to the mould. Therefore the Upilex 25S release sheets are pretreated as follows. The films are laid down side by side on a clean and dust free surface. The top side is first cleaned by dry wiping in one direction in parallel lines with a dry cloth. To remove residue and oils the film is wiped once with a paper cloth that has been wetted with IPA, the film is then allowed to dry for five minutes. Afterwards the film is wiped again but with Marbocoat 227-CEE and then allowed to dry for five minutes, this step is repeated once more.

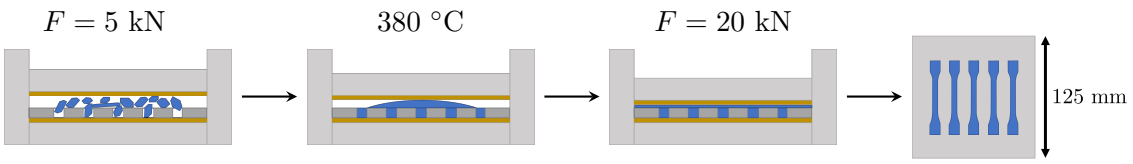

Figure 3.5: Moulding process for the dogbones

The mould is filled in the following order. First the upilex film with the coated side facing up is placed at the bottom. Followed by the mould plate, upon the mould plate the polymer chips are placed on top of the area that contains the specimen cavities. The second upilex film is placed with the coated side facing down. Then the mould is closed by placing the top plate on

the stack. The thick top plate falls within the rest of the mould, a plate stack of atleast 21 mm is used to allow the press a full stroke without bottoming on the mould edge.

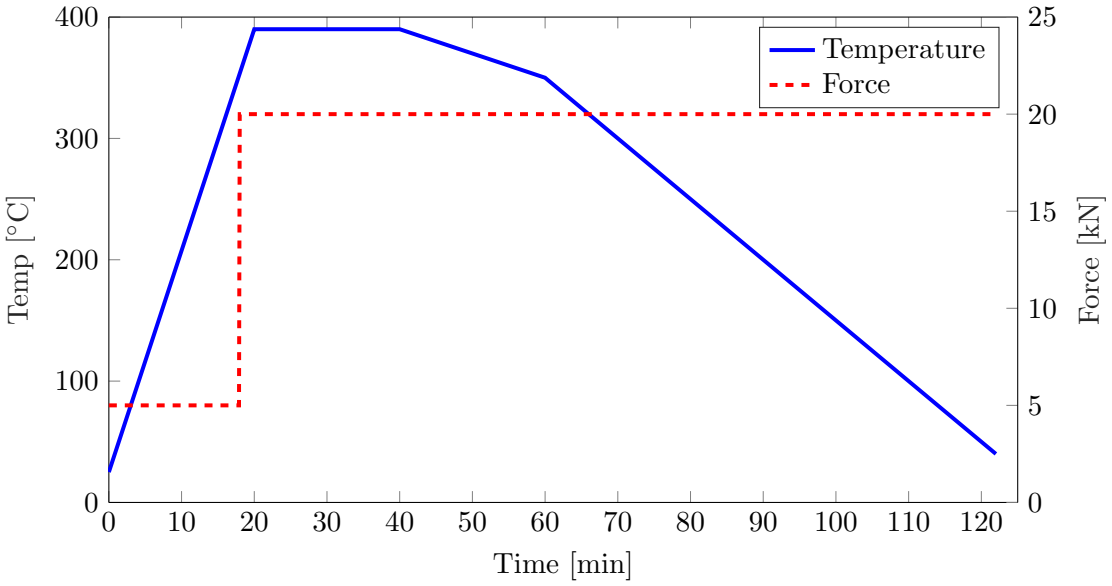

Figure 3.6: Press programming cycle

Processing is performed in a Fontijne LabPro 200 prototyping press with a plate size of 225x320 mm a maximum force of 20 kN. With a thermal ceiling of 400 °C. The thermal cycle uses slow cooling and is presented in figure 3.6. The mould is closed with 5 kN for a pressure of 3 bar and heated at 20 °C/min. At 380 °C the force is increased to 20 kN creating a pressure of 12.8 bar in the mould to completely fill the mould cavity afterwards, this temperature is sustained for 20 minutes is set. Cooling is performed at 2 °C/min until 350 °C after which a cooling rate of 5 °C/min is maintained.

Tensile specimen inspection

The specimens are then inspected for visual defects and measured using a MITUTOYO micrometer. A measurement is taken at six fixed locations for each specimen, the measurement averages are presented in table 3.3. The thickness, width at the middle of the ends and width in the gauge length are all measured at either ends of the gauge length. Nearly all samples conformed to the tolerance set by the ISO standard, but more critical is the spread of the measurement. The standard deviation of the measurements is only 0.025 mm for the width in the gauge length and 0.035 mm for the thickness.

Table 3.3: Sizes of the Dogbone specimens after moulding, all sizes in mm according to locations seen in 3.7

	D1	D2	B1	B2	H1	H2
ISO spec [29]	10 ± 0.5	10 ± 0.5	5 ± 0.5	5 ± 0.5	2 ± 0.1	2 ± 0.1
Average	9.857	9.826	4.910	4.903	1.944	1.947
max	-0.037	-0.100	-0.014	-0.016	0.008	0.048
min	-0.198	-0.226	-0.132	-0.128	-0.109	-0.149

Figure 3.7: Example of a moulded dogbone specimen according to ISO 20753-12A

3.2.4 Film specimens

The PEKK/GNP blends were placed in a flat mould, which is illustrated in figure 3.8. A flat steel plate of 250x250mm is used upon which a sheet of upilex 25S is laid as a solid release agent. In the middle of the plate a pile of 2.60 g is placed in a circle of 5 cm. Around the perimeter of the plate strips of 25 mm upilex RN50 are placed to provide an end to the flow path and limit the flow channel to around 50 µm. To finish the mould another sheet of upilex 25S is placed on top after which the top plate is laid on. This package is placed in the fontijne LabPro 200 press that was also used to produce the dogbone samples. The press is closed and set to a force of 20 kN, which equates to a pressure of 10 bar if divided evenly over the whole area. The package is then heated to 390 °C at 20 °C/min, at the upper temperature a dwell time of 10 min is set to allow the material time to flow. The material is then cooled down at an average rate of 5 °C/min.

Figure 3.8: Film mould before entering the press

3.3 Characterisation methods

3.3.1 Crystallographic characterisation

A Keyence VHX 7000 optical microscope combined with a Linkam THMS600 hot stage is used, the setup is presented in figure 3.9. For the hotstage the temperature indicated is corrected using the following formula:

$$T_{real} = 0.9531 * T_{set} + 1.0447 \tag{3.1}$$

Linkam glass slides of 16mm in diameter with a thickness of 150 µm are used. These slides envelop the molten polymer in a sandwich construction. By pressing the glass slides together the polymer can be spread out sufficiently to create a very thin layer. The combination allows the

direct observation of the polymer through a temperature profile set in the Linkam software. In hotstage optical microscopy every 20 seconds an image of the polymer melt is captured during non-solthermal cooling at 5 °C min down from 400 °C.

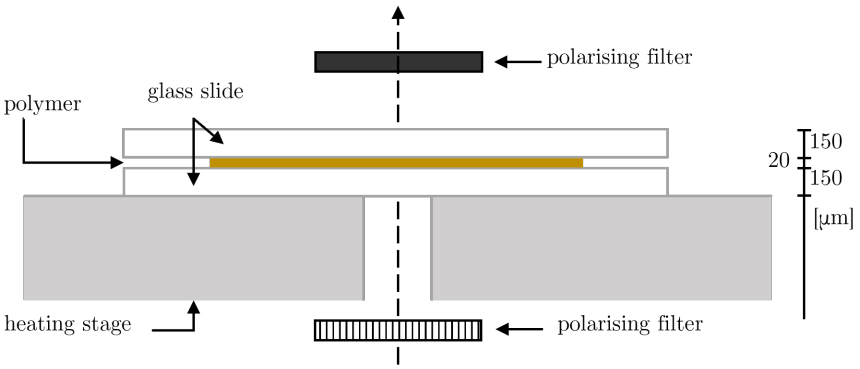

Figure 3.9: Setup used for hot stage microscopy

Large sample hot stage procedure

For analysing the homogeneity of the nucleation field the typical HSM procedure is restrictive in it's field of view. Therefore a second method is developed where the hot stage is used to monitor the polymer melt until the start of nucleation, after which the sample is removed from the hotstage and quenched in a beaker of water. This enable imaging of the nucleation field at room temperature without the hotstage. As the action of quenching freezes the status of the crystallisation process it is important to take a consistent point in this transient process. For that purpose DSC results are used. Every sample is removed from the hotstage during the cooling process at 10 °C below the onset of crystallisation temperature found through DSC. The complete thermal cycle can be seen in figure 3.10. In testing 2 to 3 mg of PEKK/GNP powder

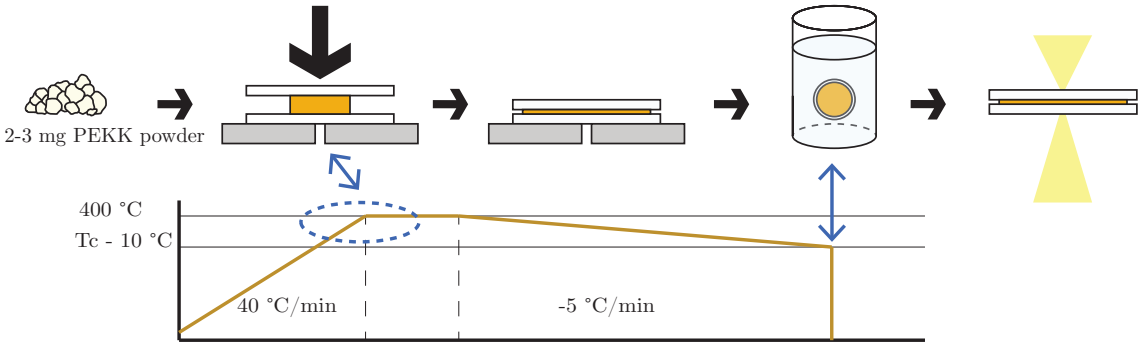

Figure 3.10: Hotstage thermal cycle

is placed in the middle of the glass slide on the hotstage and the second cover slide is placed on top. Heating to 400 °C is done at 40 °C/min. Once the polymer is molten it is spread out by pressing the glass slide with a spatula until the melt is nearly translucent and covers most of the slide. A dwell is set at 400°C for five minutes to remove the thermal history. The polymer is cooled at a constant rate of 5 °C min until $T_c - 10$ °C. Then the slide is removed from the hotstage and immediately quenched in a large beaker of water. After the nucleation field is frozen it is imaged at 300x magnification using a stitched image with a resolution of 0.53 µm per pixel.

Image analysis of nucleation field

For further numerical analysis of the nucleation homogeneity of the polymer the crystal nucleus locations need to be extracted from the image. The image analysis is performed in MATLAB. The goal of digital image analysis here is to extract the x-y locations of the nuclei in the sample. Using these coordinates the distribution will be analysed. In figure 3.11a the start point and end of the image analysis can be seen including two intermediate steps.
First the nucleation field image is preprocessed by setting the background and defects such as small bubbles or a crack in the image to zero luminance. The image is then imported in MATLAB and converted from RGB to a greyscale image. Using the unsharp masking method with a radius of 2 pixels the image is sharpened. In some samples a global gradient is present with one side appearing brighter than the other. In these situations global thresholding with a fixed value is not sufficient as in dark area's the threshold will be too high and sites of interest will be missed and vice versa for bright areas. To combat this effect an adaptive threshold is used with zones the size of $\frac{1}{64}^{th}$ the image size. This adaptive map contains a slightly different threshold value for each pixel in the image. The image is then binarised using this pixel specific threshold, visible in image two of figure 3.11b.
The binary image is as the name implies fully binary and thus contains no granular information any more. In the thresholding operation noise can be picked up as signal, to reduce this effect areas smaller than two connected pixels are removed as this is below the visible nucleus size. Under a polarised light microscope a polymeric spherulite is not directly visible but a typical Maltese cross produced by the diffracted light is visible [11, 25]. In thresholding this cross is typically split in four distinct regions. To connect these structures the image binary is first dilated by four pixels. To return to the original separation the image is then eroded by the same amount. The end result is a binary image where each island of one values corresponds to a crystal nucleus in the image, which can be seen in image three of figure 3.11c. X-Y coordinates are calculated using the matlab *regionprops* function where each point is taken as the weighted centroid of a pixel blob.

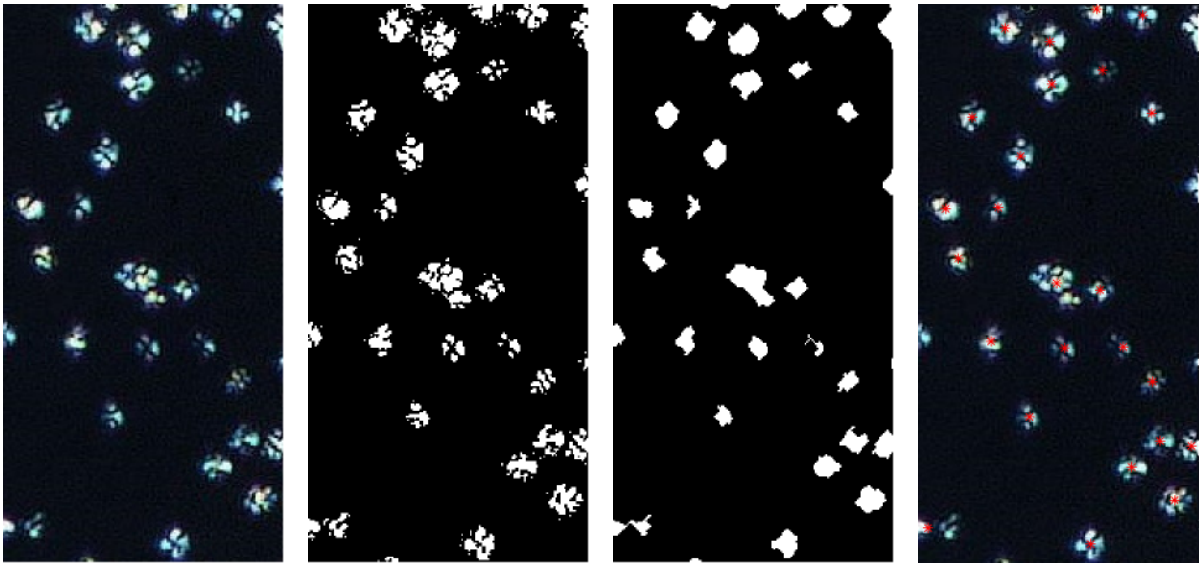

(a) HSM image (b) Binary image (c) Processed image (d) Crystal location (red)

Figure 3.11: Image processing showing intermediate steps

Analysis of the nucleation density field

Quantifying the homogeneity of the nucleation field requires a metric. In polymer research typically a diameter of the spherulites is used to indicate the crystal size. As the hotstage images only show a nucleation field and not a fully crystallised bulk the spherulites that could have been created from this field are to be estimated. Once nucleated a spherulite shows radial growth. The growth rate is predominantly dependent on temperature [11]. As all the nuclei are approximately at the same temperature the growth rate is not a factor that influences the crystal morphology. Therefore a Voronoi diagram is used [11]. Voronoi diagrams subdivide an area in to regions. These regions have the property that they contain part of the area where it's point is closest. A boundary between two of these regions is defined by two points is a perpendicular bisector between these points.

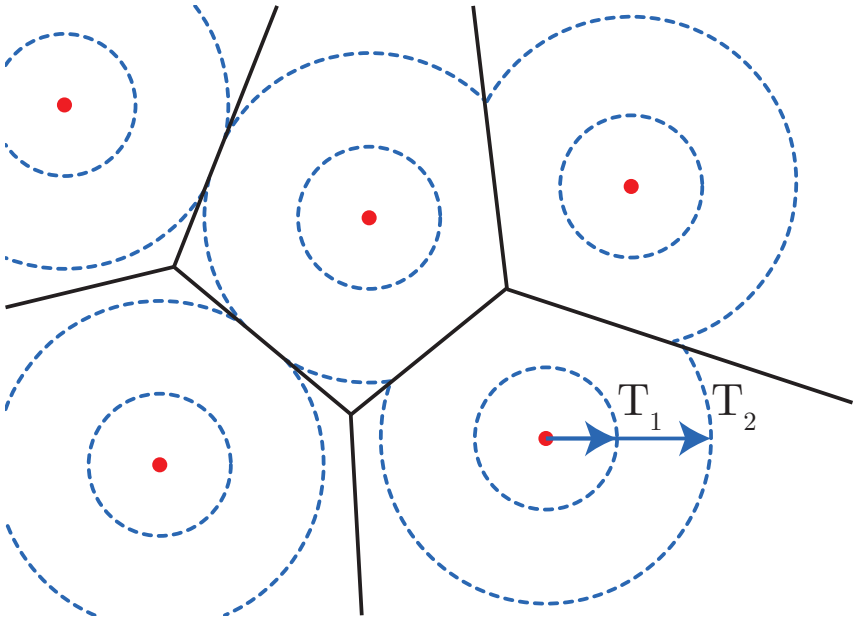

Figure 3.12: Illustration of theoretical spherulitic growth with nucleation sites in red and crystal boundaries at two points in time in blue.

In a MATLAB script the nucleation field from the image analysis is imported and analysed using the *voronoin* function. For each nucleus a corresponding voronoi cell is calculated resulting in the vertices of each cell. Calculating the area of each cell is accomplished by using the trapezoid formula which can be used for irregular non intersecting polygons.

$$A = \frac{1}{2}\sum_{i=1}^{n}\left(y_i + y_{i+1}\right)\left(x_i - x_{i+1}\right) \tag{3.2}$$

For some visualisations it is much more convenient to represent the crystal size using only one number. In those case the estimated crystal size is calculated as the diameter of a circle with the equivalent area.

$$d = \sqrt{\frac{2A}{\pi}} \tag{3.3}$$

Another method that is used often in literature for describing the nucleation field is the nucleation density parameter $N0$. This parameter describes the amount of nuclei per volume of polymer and is calculated by dividing the amount of nuclei by the analysed volume:

$$N0 = \frac{number\,of\,nuclei}{analysed\,volume\,[\mu m^3]} \tag{3.4}$$

3.3.2 Thermal characterisation

For the DSC analysis a TA DSC 250 with auto sampler is used. Subsequent data analysis is performed using the associated software package TRIOS also provided by TA instruments. For the full analysis of the polymer material blends made the following properties were characterised using the following settings:

Melting point T_m, From the data the melting point is taken as the peak in the endotherm. **Crystallisation temperature** T_c, the crystallisation temperature is taken as temperature corresponding to the peak in the exotherm. The onset temperature is found in the software by finding the intersection between two lines, the baseline and the linear part of the cooling peak. **Crystallisation time** t_c, the kinetics of the crystallisation process are characterised in the crystallisation time. The width of the exothermic peak is evaluated at half the maximum value. **Enthalpy of fusion** ΔH, to integrate the melting peak a baseline is required. To that end a linear baseline is used from 200 °C until 380 °C which is used often in literature [15]. **Relative crystallinity** x_c, determining the fraction of the polymer in a crystalline state is accomplished by comparing the specific enthalpy of a fully crystalline sample to the specific enthalpy in the polymer that is evaluated. These fully crystalline melting enthalpies are found by analysing the unit cell of crystal and extrapolating the density of a perfect crystal structure. For PEEK this results in a specific heat of fusion ΔH of 130 kJ/kg [7].

$$x_c = \frac{\Delta H}{\Delta H_{100\%}} \tag{3.5}$$

For this research the DSC was mainly utilised to analyse the crystallinity present in the PEKK polymer. Every polymeric sample that was analysed went through the following thermal steps:

- Equilibrate at 40 °C
- Ramp to 390 °C at 10 °C/min
- Isothermal for 3 min
- Ramp to 40 °C at 5 °C/min
- Isothermal for 1 min
- Ramp to 400 °C at 10 °C/min
- Isothermal for 1 min
- Ramp to 40 °C at 10 °C/min

DSC scans are performed from ambient temperature to a temperature above T_m. In this range both the glass transition and melting behaviour can be analysed. The analysis consists of two cycles, the first to remove thermal history and volatiles, the second for data collection. Between each step a short isothermal period is set such that DSC controller has some extra time to switch to the next step. A cooling rate of 5 °C/min is used to simulate the same cooling condition as will be achievable in an autoclave process. A second heating scan is performed to analyse the material under heating conditions and validate the crystallinity found under cooling. On the last cooling scan the material is cooled again to ambient temperature. In this scan the T_g value is compared to check if degradation occurred.

3.3.3 Mechanical evaluation of nano-composites

Determining the material properties of a material can be performed using a plethora of methods which all vary in their specific strengths and weaknesses. In the research question the goal is

to homogenise the crystalline structure, therefore a macroscale evaluation method is used. A reduced scale dogbone shape 12A is used from the ISO 20753:2018 norm [29]. With a gauge length of 30 mm, 5 mm width and 2 mm thickness the 12A shape (named 1BA in older norms) this shape has sufficient material to be tested. The specimen volume is 1038 mm^3 resulting in a material consumption of 1.34 g per specimen.

Tensile test setup

The experimental setup for the tensile tests can be seen in figure 3.13. The tensile tester used is a Zwick/Roell Z100, which is equipped Zwick/Roell 8506 wedge grips. In this tester the loadcell is located between the machine frame and the bottom clamp. The loadcell is a GTM GMBH NR. 20737 100KN cell. Testing is performed at a test speed of 25 mm/s.

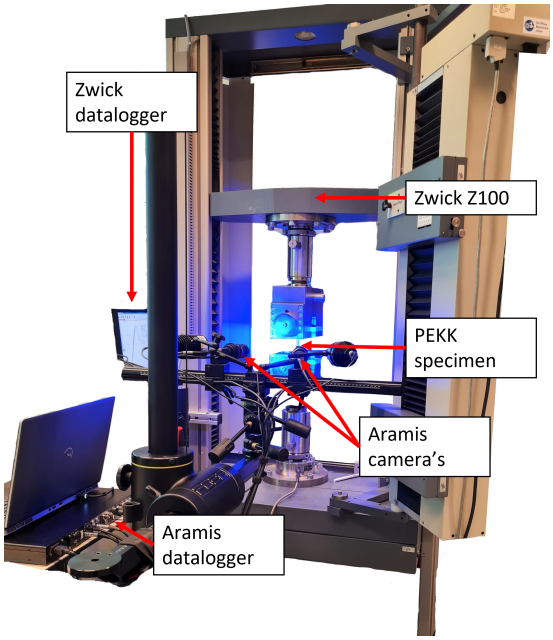

Figure 3.13: Tensile testing setup

Strain measurement system

Strain is externally measured using an optical DIC (Digital image correlation) installation, an Aramis adjustable camera setup produced by GOM. Cameras record the surface of a sample and using facet tracking the distortion of that surface is calculated. Using this optical method to measure the deformation field of the samples both the engineering strain and the local strain in the specimen can be measured. To get a good signal a high contrast pattern is required on the samples. To accomplish this the dogbone specimens are first protected using masking tape which covers the gripping area of the sample. Then sprayed with a white satin base coat, after 10 minutes the black speckle pattern is painted on using graphite paint which is sprayed from 50 cm distance to the correct speckle density. The resulting dogbone with speckle pattern can be seen in figure 3.14.

Data analysis

The output produced from the Aramis software is a strain field containing around 3000 evenly distributed points for every time instance that is captured. Sample frequency for the system

Figure 3.14: Dogbone specimen with speckle pattern

is limited by the data throughput so the frame rate is set at 20 Hz. The signal alignment is explained in the appendix in section A. For presentation in figures and calculations the aramis signal is linearly interpolated to the faster sampled signal from the tensile tester. A strain signal is also determined from the strain field, this is created by averaging over the strain field values that lie within the gauge length of the sample. Next to that also a maximum strain signal is made by averaging over the 20 largest strain values within the gauge length.

3.3.4 Fracture surface analysis

To evaluate the failure mode that occurred in the polymer on a micro scale the scanning electron microscope (SEM) was utilised. The electron microscope utilised for imaging is a Thermofischer Phenom XL. This microscope has a large holder for samples up to 100x100 mm and uses a backscatter detector. The large sample size allows the placement of the broken dogbone specimens in their entirety. PEKK polymer is an insulator and thus will collect charge from the electron beam. To mitigate this effect and make the production of sharp images possible the specimens are sputter coated with a thin layer of gold with a JEOL sputter coater for 120 seconds. For imaging a medium atmosphere setting of 10 Pa with an acceleration voltage of 10 to 15 kV.

4 RESULTS

4.1 Crystallisation - nuclei distribution

The results of the hot stage microscopy analysis will be discussed in the chapter. The aim is to evaluate and analyse the nucleation field in PEKK and highlight inhomogeneities in the nucleation field. The nucleation ability of graphene in PEKK polymer had been reported before by [19, 16], in the results presented this effect is once confirmed and further effects that graphene has on the nucleation and crystallisation kinetics are reported.

(a) 0 wt% GNP (b) 0.01 wt% GNP (c) 0.05 wt% GNP

Figure 4.1: 530x530 μm image of the nucleation field in PEKK at $T_c - 10°C$

In figure 4.1 the effect of adding GNP to the polymer melt is visualised. Here figure 4.1a shows the natural nucleation field of the PEKK polymer without any GNP. The visible nuclei are spaced quite far apart and show no regularity in the locations. With the addition of 0.01 wt% GNP, the nucleation field becomes considerably denser in figure 4.1b. Increasing the amount of GNP to 0.05 wt% does increase the density of the nucleation field slightly in figure 4.1c. The limited scale of these images hides many defects in the nucleation field. To that end a method for creating larger slides of the PEKK nucleation field was developed as described in section 3.3.1. Through the employ of this method, many regions can be found in the sample containing GNP whose nucleation density was almost unchanged, as displayed in image 4.2. These areas of low nucleation density which are assumed to have lower GNP content, are significantly different from the bulk and thus pose an inhomogeneity in the mixed material.

To quantify the homogeneity of the material and the diversity of crystal sizes the quenched HSM slide method is used. Previously areas of 0.161 mm^2 could be analysed at a time, the size of which is illustrated in figure 4.2(b) against a slide made with the new method. These slides contain usable areas up to 53 mm^2. Providing a much broader view of the material, which enables the evaluation of the homogeneity.

For consistent properties of the slides, the quench temperature was controlled at $T_c - 10°C$. The thickness of all slides is between 20 and 30 µm. Before the image analysis the central section in the slide that was on top of the hole and bubbles if present were completely excluded from the analysis. The counted number of nuclei is significantly higher in the samples that contained GNP. More interesting is the global nucleation density $N0$ which can be taken as an indication of the eventual crystal size, but is not as accurate as it relies on the thickness for the volume input which is measured after the fact. The mean size in the table is calculated using the Voronoi area method as described in the methodology. The crystal sizes in the table stem from the analysis of each Voronoi cell is a much better indicator for the crystal size. On the generated size data of the Voronoi cells, a normal distribution is fit of which the mean and the standard deviation

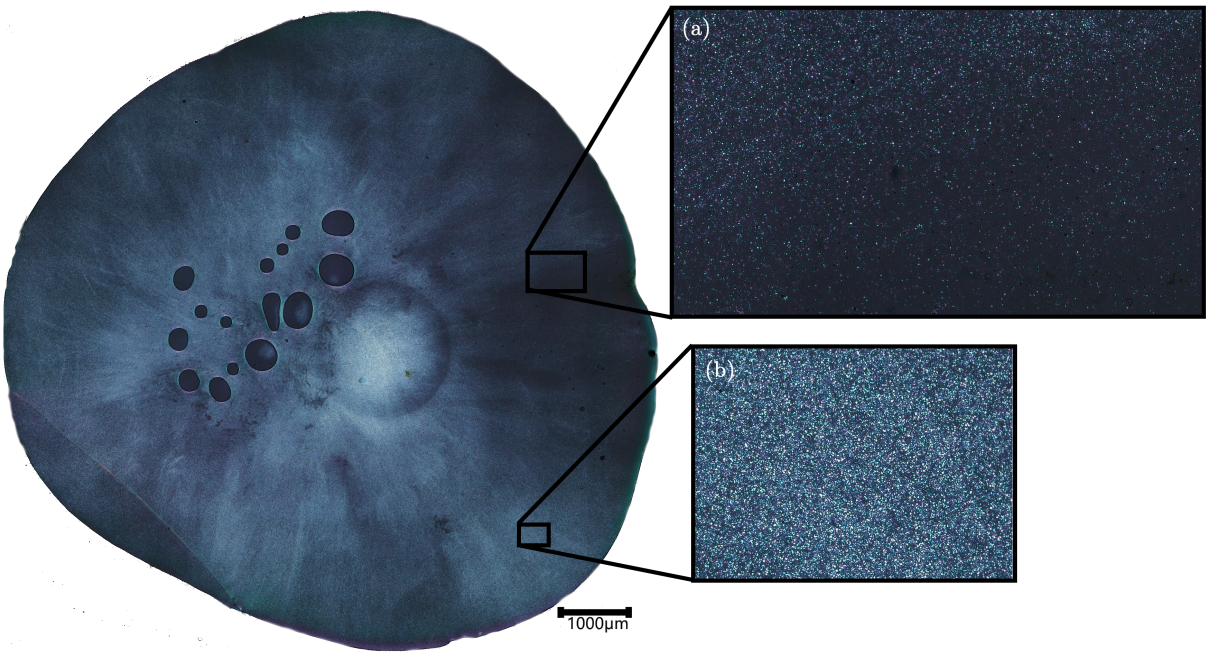

Figure 4.2: Full view of the HSM slide of the $C_{0.01}$ sample. (a) detail of section containing lower than average nucleation density. (b) section corresponding to the field of view used in previous experiments that can hide many inhomogeneities.

are presented in the table.

First, the method and assumptions as described in the methodology for estimating the crystal boundaries are validated. This method uses the nuclei coordinates that were extracted from the microscopy slides to estimate the crystal morphology using a voronoi chart. Two main assumptions are made for this analysis. It is assumed that at the quenching point in time all the nuclei that will contribute to the crystallisation are already present. For the heterogeneously nucleated samples, this assumption is quite safe as nucleation happens in a very short period. For the PEKK samples without GNP, nucleation occurs through homogenous nucleation which occurs over a larger period. Some stable nuclei can already form at high temperatures while some form halfway through the crystallisation process. To validate this method a time-lapse was made on the HSM throughout the cooling process. The transient crystallisation process is shown in figure 4.3 with an overlay of the estimated crystal boundaries from the nuclei positions.

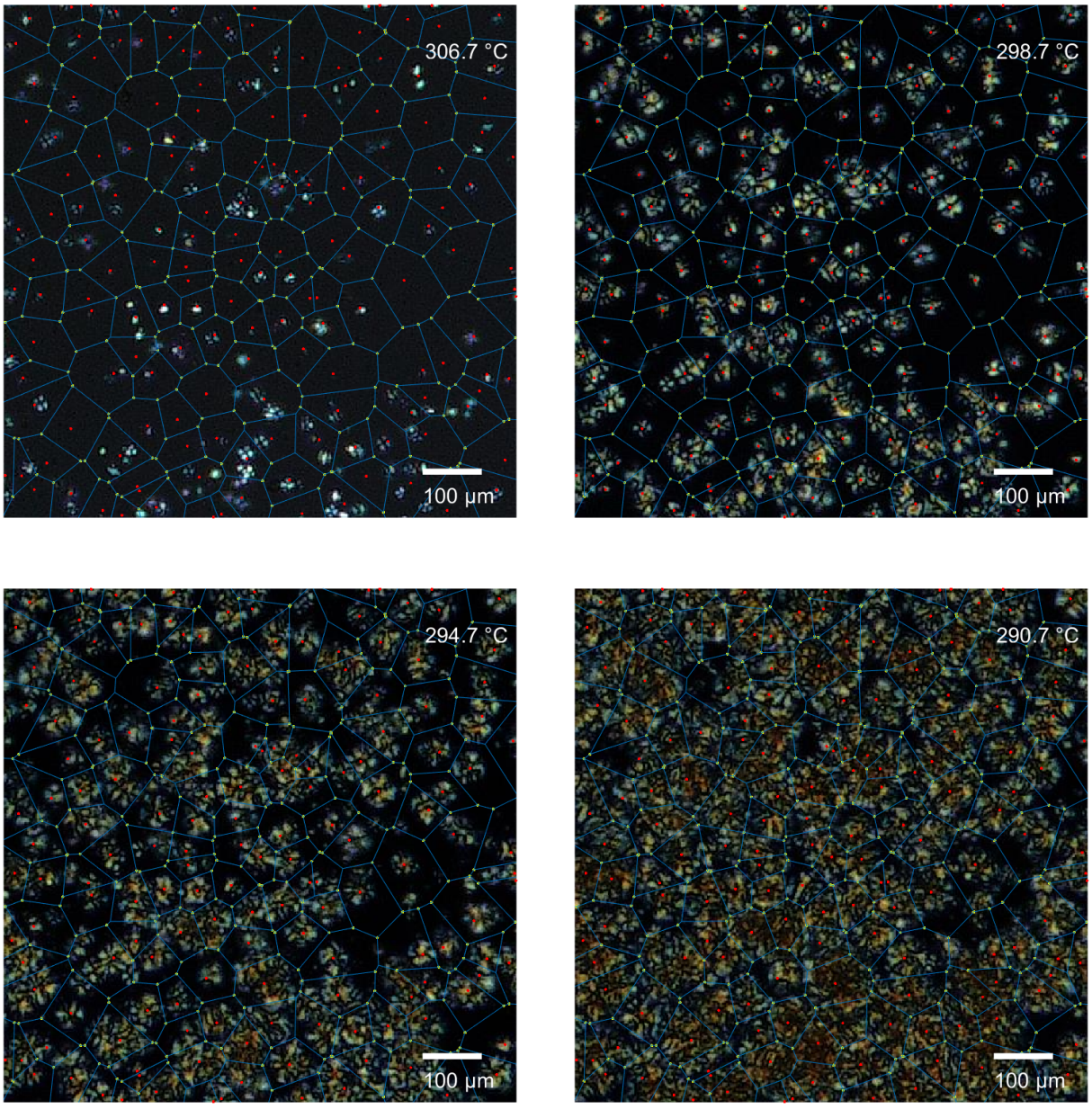

Figure 4.3: Cooling crystallisation of homogeneously nucleated C_0 PEKK with an overlayed with the nucleus locations from image recognition in red, the voronoi area's in blue and their vertices in yellow.

In the cooling process, the crystal growth lines up well with the predicted boundaries. However, two types of deviations are present. Contrary to the assumption made some nuclei form after the initial image used for the nuclei analysis. The effect on the results is that a few more crystals exist than estimated, resulting in a slight over estimation of the crystal size. The other short coming of the method is that at $T_c - 10°C$ the nuclei are assumed to be the same size as only the locations are used for the estimation. In the presented figure this is not the case everywhere but the number of nuclei missed is negligible. The most important mitigating factor is that in these errors only typically arise in the homogeneously nucleated case. For heterogenous nucleation that is promoted by the incorporation of GNP these errors are negligible due to the short time frame that heterogeneous nucleation occurs in.

The results of the quenched HSM analysis is presented in figure 4.4. Here the crystal morphology and the distribution of their sizes are quantified. First it is clear to see that the natural crystal size of PEKK under a cooling rate of 5 °C/min is around 40 μm for PEKK. The four samples that were nucleated using GNP showed different results. With a concentration of 0.01 wt% the mean crystal size is 9 ± 2.1 µm for the coarse powder and 8.5 ± 2.4 µm for the homogeneous powder. With a higher GNP concentration, the crystal size decreases further to 7.3 ± 2.1 µm for grade C and down to 6.8 ± 1.3 µm for grade S.

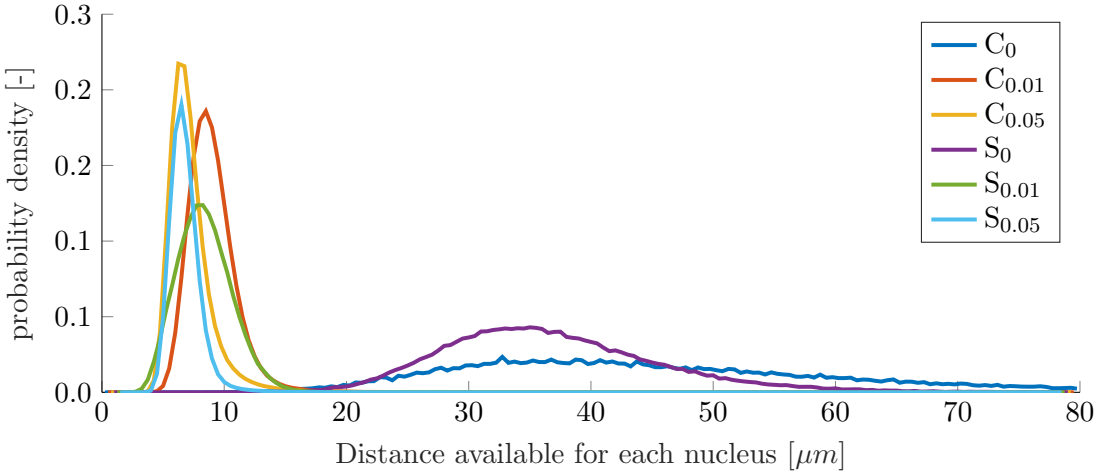

Figure 4.4: Distributions of span available for the nuclei present in the samples

There is a distinct relation between an increase in the GNP concentration in the polymer and a higher nucleation density with a smaller crystal size as a result. In table 4.1 also the shape parameter of a normal distribution fit to the crystal size data is presented. This shape parameter represents the width of the normal distribution. The samples made with the sieved powder fraction show a tighter shape parameter except for $S_{0.01}$.

Visually the samples contained distinct area's of inhomogeneity in the Grade C PEKK blends as shown in figure 4.2. Due to a large amount of data these areas are not very noticeable in the total distributions. However, with this large amount of data, it is possible to filter to only the 1 % largest estimated crystals. That is when these differences become more visible in the data. This section of the total data is shown in a cumulative histogram in figure 4.5. In the figure an extra vertical line is shown that corresponds to the average crystal size in a homogeneously nucleated sample. Any crystal sizes found above this line can still be nucleated by GNP but did not have close neighbours to impinge against. The two samples that show very similar behaviour are the samples containing 0.01 wt % GNP. The $C_{0.05}$ blend shows many outliers with much larger crystal sizes which indicate regions of low nucleation density. Where the $S_{0.05}$ polymer blend shows no outliers larger than the typical size in homogeneous nucleation. Essentially meaning no portion of the material that was completely unaffected by the GNP nucleation agent.

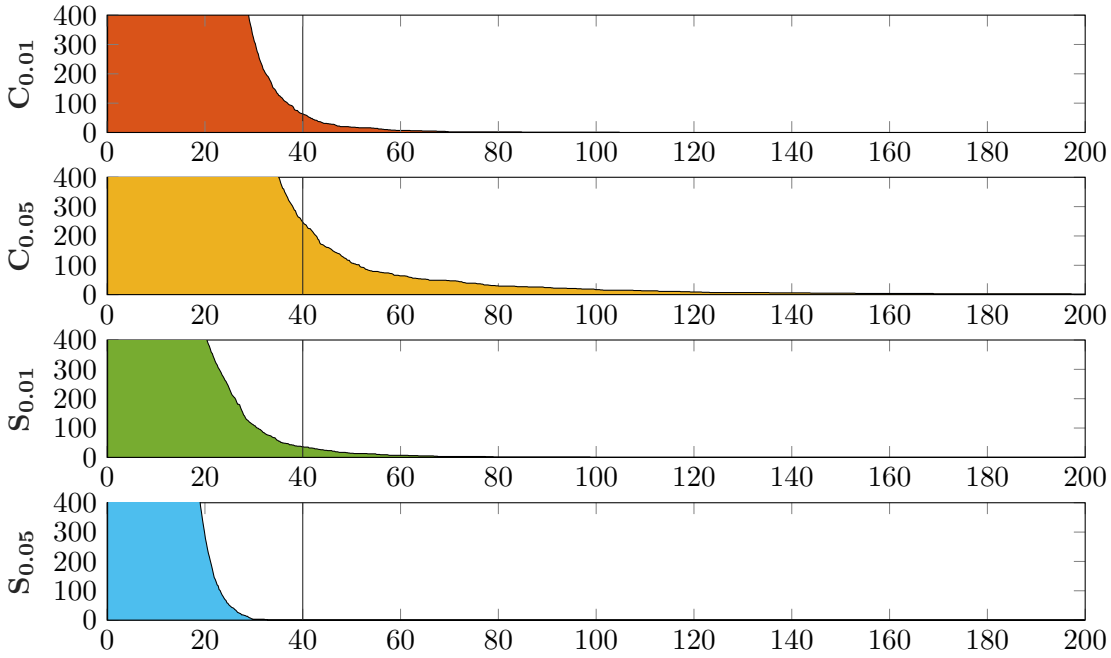

Figure 4.5: Cumulative count of the span available for crystallisation for the largest 1 %

The resulting slides are presented in table 4.1. This table contains the most important properties of the microscopy slides as well as the resulting global properties of the nucleation field. Distributions shown in figure 4.4 were fit using a normal distribution the average of which is presented in the table as the mean size and the std is the shape parameter.

Table 4.1: HSM slide properties and summarised results

Sample	weight [mg]	area [mm^2]	Quench temp [°C]	t [μm]	Nuclei [#]	N0 [# µm^{-2}]	mean size [µm]	*std*
S_0	1.94	46.51	281	25	78803	0.001596	36.7	8.9
$S_{0.01}$	2.8	53.24	289	26	566994	0.008973	8.5	2.4
$S_{0.05}$	2.33	27.50	293	31	1577180	0.050597	6.8	1.3
C_0	2.43	38.02	285	21	35926	0.000901	46.1	17.6
$C_{0.01}$	2.3	48.43	291	28	1350993	0.026112	9.0	2.1
$C_{0.05}$	2.5	52.39	297	20	2369309	0.042565	7.3	2.1

4.2 Crystallisation - thermal kinetics

In this section, DSC is used extensively to characterise the thermal kinetics of the crystallisation process in the PEKK/GNP polymer blends. The effect of heterogeneous nucleation can be indirectly observed and quantified using this method. For heterogeneous nucleation the addition of alien material to the polymer must lower the energy barrier working against the formation of nuclei [14]. Therefore in the case of nucleation with GNP, an earlier onset of the crystallisation is to be expected on the cooling scans.

4.2.1 Powder properties

In DSC testing various properties were measured as described in the methodology. First the powders were characterised after production. From the DSC testing the glass transition temperature was measured as 155 ± 0.2 °C for all the six polymer powders, the full properties of the powders can be seen in 4.2. Which is slightly lower than the glass transition specified by

Arkema [1] at 162 °C but closer to values cited in literature [23, 18, 15] . The melting temperature was 335 °C across all samples which is in direct agreement with the data from Arkema and as expected for a PEKK with a 70/30 T/I ratio. These measurements show that the base polymer is the same or at least very similar in thermal properties across the board.

Table 4.2: DSC results from the blended powders

	Tg [°C]	Tc [°C]	Tm [°C]	ΔHm [J/g]	Xc [%]	peak width [sec]
S_0	156,4	281,1	336,1	43,8	33,7	139,8
$S_{0.01}$	155,6	293,0	336,5	46,4	35,7	96,6
$S_{0.05}$	154,9	295,1	336,4	46,7	35,9	104,9
C_0	156,2	267,9	334,7	43,9	33,8	168,0
$C_{0.01}$	155,5	291,7	335,8	44,2	34,0	139,0
$C_{0.05}$	155,7	294,9	337,1	44,1	33,9	135,9

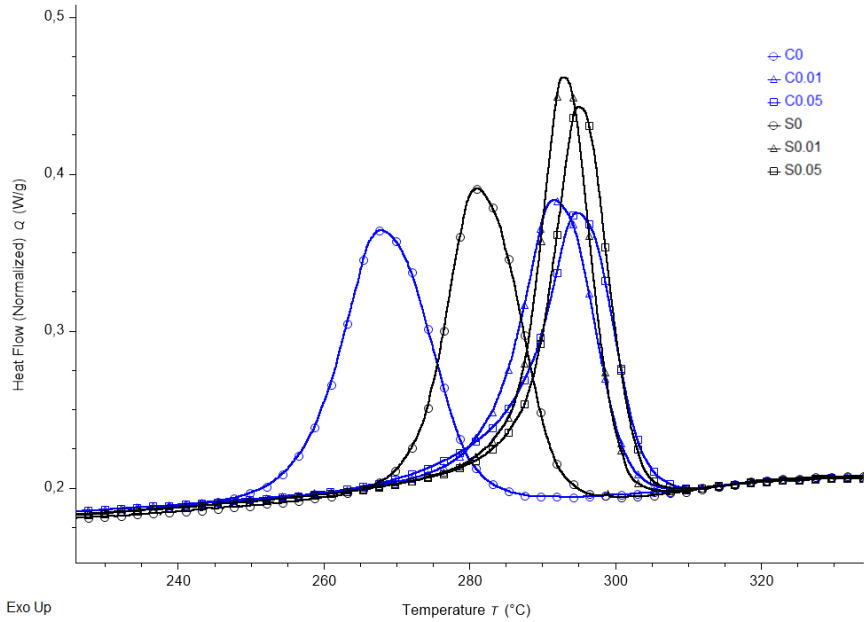

Figure 4.6: Second cooling normalised heat flow from the powder samples

Distinctions arise in the melting enthalpies and the crystallisation process. The results from the cooling scans of the DSC process as described in section 3.3.2 are presented in figure 4.6. In the temperature window of 320 °C to 300 °C the PEKK powders that went through the GNP mixing procedure start crystallising at higher temperatures. These T_c peak and onset temperatures are graphed in figure 4.7. Due to the addition of GNP, stable nuclei can be formed at higher temperatures and the onset temperature increases. The onset temperature scales quite well with the $wt\%$ GNP for all samples. For the Grade C samples the onset temperature was highest by a small margin, which is most likely due to small areas of with a very high GNP density. From 300 °C to 290 °C the peak is wider and less tall in the grade C samples than the grade S samples. Due to the more homogeneous distribution as shown with the HSM experiments, the spacing between nuclei is very even so the crystal growing fronts impinge at nearly the same point in time. In a less homogeneous sample, the growth fronts need to travel further in some areas and shorter distances in others. This variation spreads the peak out. The crystallisation is quite different between the two different PEKK powders that contain no GNP. These samples crystallise by homogeneous nucleation, thus their crystallisation temperature is

mainly a function of chain mobility, chain orientation and possible contamination. Most likely the smaller polymer particle is either more oriented, decreasing the difference in entropy to the crystal form. Another option is that this polymer is of a slightly lower molecular weight, increasing chain mobility.

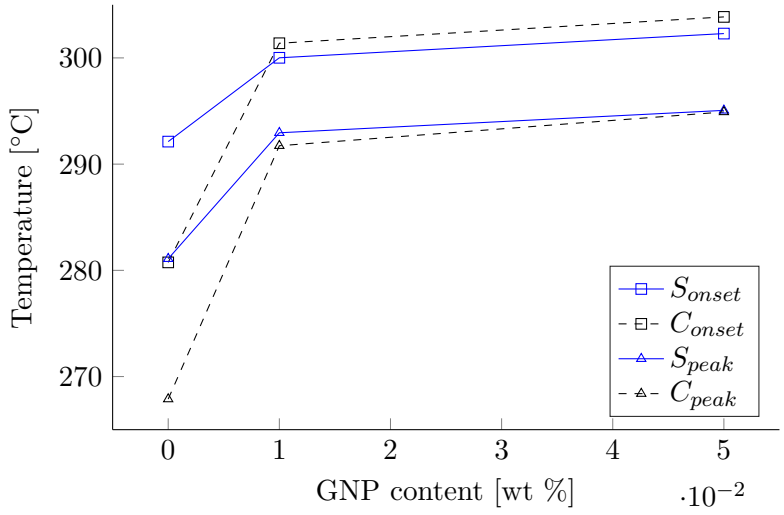

Figure 4.7: Peak and onset temperatures of crystallisation

4.2.2 Effect of melt mixing

To test the effect of shear mixing on the thermal properties of the polymer samples were subjected to shear by flowing through a small channel. The peak widths of the materials were quite spaced in powder testing. After the radial flow, the peak widths of the processed polymers are almost identical between the sieved and the Grade C powders.

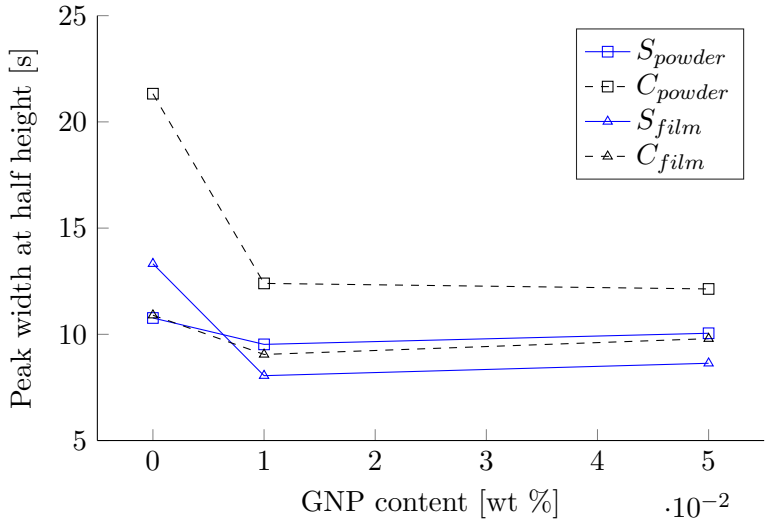

Figure 4.8: Crystallisation peak width in minutes

Interesting to note is that the polymer powders without any GNP show a very similar crystallisation behaviour compared to the DSC results from the powder tests. These polymers went through the same process so the local orientation of the chains is also similar. The radial flow created by the pressing process is similar to the typical extensional flow condition that increases the chain alignment and thus decreases the entropic difference to the crystal form. From this

result it is possible to say that the difference between the polymers present in powder testing was due to the processing history and not a difference in composition.

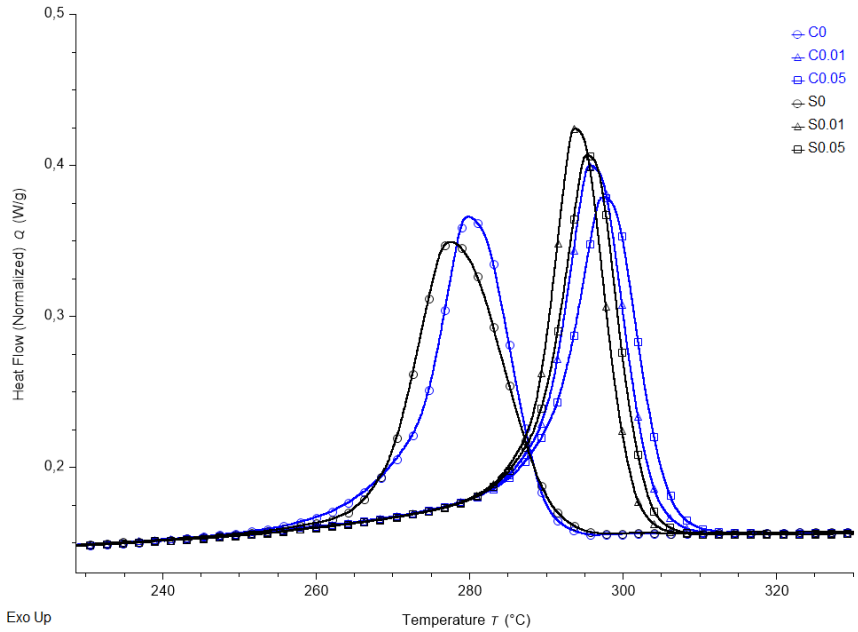

Figure 4.9: Second cooling normalised heat flow from the powder samples

4.3 Discussion - crystallisation

Two main methods were employed to attain a thorough understanding of the crystal morphology present in the PEKK blends containing GNP and pure PEKK samples. The quenched HSM experiments allowed the observation of large areas of the nucleation field. Combined with the proven thermal characterisation method of DSC providing insight into the crystal growth kinetics under the same thermal conditions as in the HSM. Hot stage microscopy showed the density of the nucleation field, which is the starting point for crystallisation. With DSC the growth of this field can then be further evaluated.

The nucleation parameter N0 is used in literature but not many values for PEKK are reported. Values found in this research, $6.88 * 10^{-5}$ µm^{-3} for Grade C and $4.5 * 10^{-5}$ µm^{-3} for Grade S are close to the values found using the number of active nuclei model reported by Koscher et al [30]. Using the parameter values of Chelaghma et al. [11] for the homogeneously nucleated samples the model predicts a nucleation density of $1.4 * 10^{-5}$ µm^{-3}. Choupin et al. also determined N0 but for the isothermal case at 270 °C, reporting $1.4 * 10^{-3}$ µm^{-3} [15]. The likely cause for the difference of the values reported by Choupin compared to Chelaghma et al. and this research is that lower temperatures were used combined with a different slide thickness. HSM is inherently a 2D method but the molten film still has some thickness. In this research the average slide thickness was measured at 25 µm, Chelaghma et al. used a 40 µm film and Choupin a 5 µm film. The film thickness should be at most around the typical size of a spherulite such that the result can be regarded as a 2-dimensional slice. In this research the thickness of the molten material could obscure nuclei in dense areas, therefore making it in sufficient for determining a correct N0 value in the samples containing GNP. However for the goals of this research, identifying and quantifying areas of inhomogeneity, proved sufficient.

Generally, samples that showed inhomogeneity in the HSM tests showed wider crystallisation

peaks in DSC testing. In the samples that showed some inhomogeneity of the nucleation field the onset of crystallisation temperature was also higher. Since the onset temperature in DSC is only affected by the number of nuclei that can be formed and the temperature they can be formed at, clusters of closely packed GNP and PEKK can explain the early onset. The tail of the crystallisation peaks at lower temperatures is created when there are areas of low nucleation density where the crystal growth front needs to travel further for it to impinge against it's nearest neighbours.

However, a large discrepancy also exists in the crystallisation behaviour of the PEKK samples without GNP. This difference is present in the powder samples but disappeared in the melt mixed results. In the HSM results, the Grade C specimens also showed a lower nucleation density than the sieved samples. Indicating that the sieved powder samples are not of neutral chain orientation but in some state of alignment. As the crystallisation in these samples is nearly the same after being exposed to the elongational flow in the film processing step. Result in literature [15] the values found for the peak crystallisation temperature of the homogeneously nucleated PEKK are quite comparable and lie in the range of 275 °C which is in-between the values found for the coarse and the sieved PEKK polymer.

The addition of a melt processing step, where the material is elongated and mixed above T_m changed the DSC data significantly. This step moved the coarse PEKK blends close to the results of the sieved powders, thus showing that an increase in homogeneity can also be attained through a shear mixing step. However, the melt mixing step also slightly decreased the peak width at half height of the sieved sample, indicating further improvements to be possible beyond the current distribution.

4.4 Mechanical performance

In this section, the polymer samples are subjected to mechanical testing to evaluate the effect of the spherulite size and processing methods on the mechanical properties. In the context of a hybrid joint, it is of interest to attain a bond with a high strength but also a high toughness, toughness is typically quantified as the ability of the material to absorb deformation energy.

From previous research, the homogeneity of the material was a point of concern. In the utilised mandrel peel and DCB test setups small areas of inhomogeneity that have a more brittle response do not affect the results considerably. In the crack tip of a DCB and mandrel peel specimen, the material is subjected to a mode I loading. In the cracktip of such a mode I loadcase the material is primarily loaded under tension. To amplify the effect of these areas testing is performed using a uniaxial tensile setup.

Tensile testing was performed on the six different blends of the polymer as stated in section 2.6. Throughout processing care was taken to minimize exposure to temperatures above T_g where possible. With the described process consistent dimensions of the specimens were attained. To check for voids and weight loss the density of the samples was measured after production. Per the datasheet the bulk density of PEKK is specified as 1.29 g/cm^3 [1], the average density of the specimens was measured at 1.283 g/cm^3 with a standard deviation of 0.0011. Comparable density to the datasheet at least shows indications of low void content. From DSC testing the melting enthalpy of the dogbones samples was measured at 45 to 47 J/g resulting in a relative crystallinity of 35 to 37 % across all samples, both without and the samples containing GNP. Which is the same as the results from the powders if not marginally higher. With the crystalline content of the samples on the same level, the percentage of the sample mass that is crystalline is on the same level.

In testing the Grade C polymer and the Grade S showed different mechanical responses, which is

shown in figure 4.10. The GNP content is far too low to provide stiffness to the materials as the addition of fibres would do in a composite. The youngs' modulus is virtually the same for the samples that do contain GNP as the pure samples. There is a difference but only a few percentage points, however this difference lies within the standard deviation of the measurements.

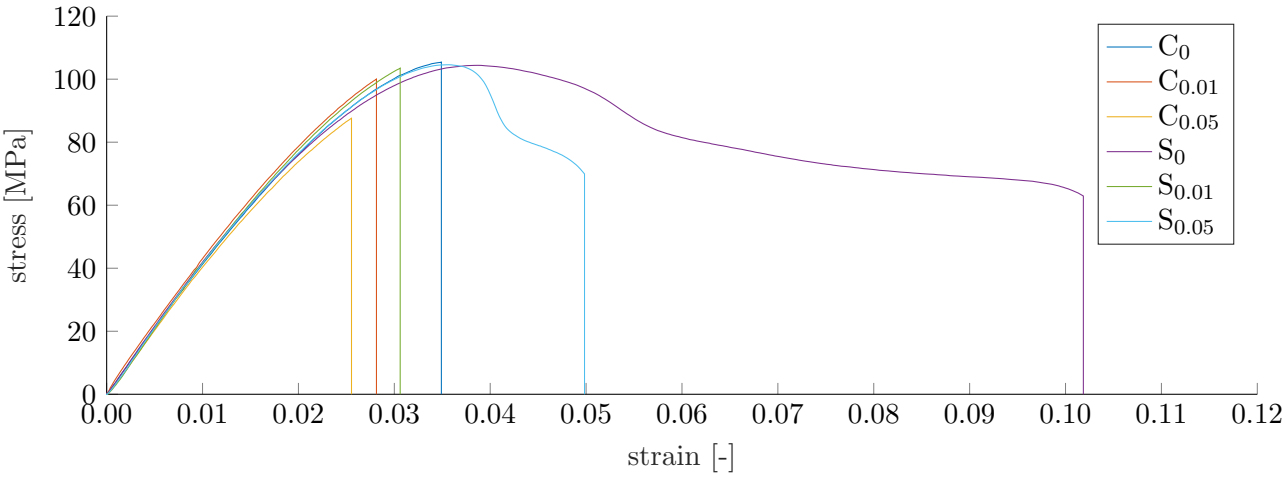

Figure 4.10: Stress strain curve of the tested samples with median ϵ_{break}

With the yielding of the samples major differences start to appear. First, many samples showed a brittle failure before the material reached its yield strength. Therefore in table 4.3 a distinction is made between the largest measured stress in a test, σ_{max} and maximum stress where the slope of the curve is zero σ_y. Generally, the sieved powder samples had a higher yield strength compared to Grade C. During testing the two polymer grades showed different behaviour. Grade C generally had a brittle response and also fractures occurred before considerable yielding in some cases. Thereby decreasing its yield strength as shown in figure 4.12b.

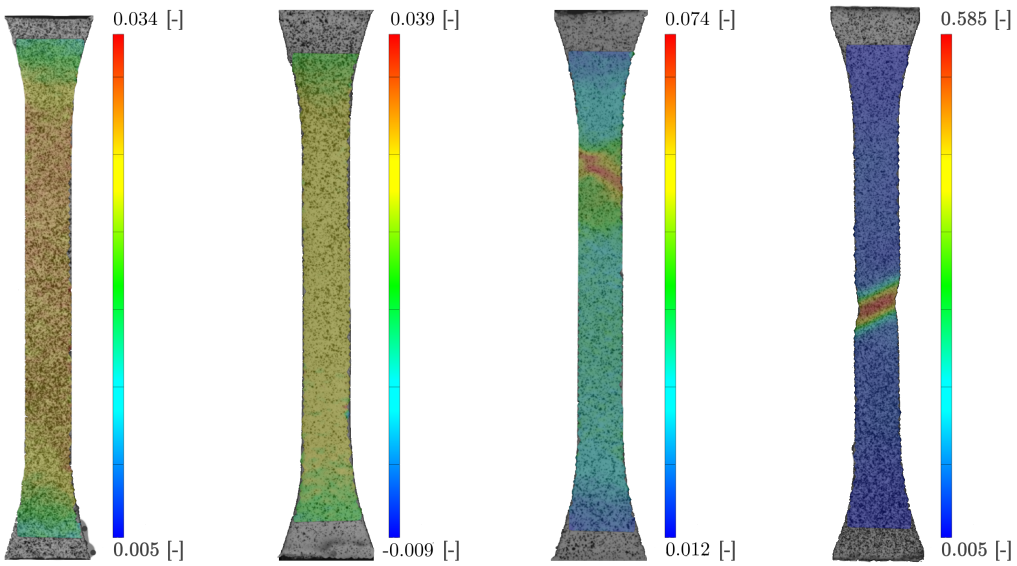

(a) Brittle fracture in a $C_{0.01}$ specimen (b) Brittle fracture in a $C_{0.05}$ specimen (c) Stress-localisation in a $S_{0.01}$ specimen (d) Ductile fracture in a $S_{0.05}$ specimen

Figure 4.11: Last frame before failure with ϵ_y overlay from DIC data

A widespread mechanical response between a fully brittle and quite ductile response. With the

help of the DIC data, it was possible to determine if any necking or localisation was happening in the sample. Typically the stress-strain curves are used for this purpose but the DIC data showed very clear differences. With the brittle failures, the strain would rise to around 0.03 while showing an even strain field at which point it would suddenly break. The ductile responses were mainly seen in the S_0 and $S_{0.05}$ sets of specimens but every set contained at least one sample that reached the yielding plateau. Ductile failures first showed localisation of the strain under a 30 to 45 ° angle. After which the amount of plastic flow varied largely between the samples. This difference is best illustrated in figure 4.12c where the energy that is absorbed by the specimen during testing is visualised. Every sample absorbed at least about one J as that is still in the elastic loading phase. Samples that consumed more than two J showed much more energy absorption with the highest results around 4.5 to 5 J for some S_0 and $S_{0.05}$ samples.

Table 4.3: Results of mechanical testing

sample	E [GPa]	std	σ_{max} [MPa]	std	σy [MPa]	N_{duct}	ϵ^{eng}_{max} [-]	ϵ^{loc}_{brmin} [-]	ϵ^{loc}_{brmax} [-]	work [J]	std
C_0	3.81	0.11	96.83	19.12	106.38	3	0.053	0.045	0.529	1.514	0.676
$C_{0.01}$	3.95	0.07	99.21	12.39	108.29	1	0.031	0.025	0.047	1.272	0.382
$C_{0.05}$	3.88	0.06	94.88	10.89	109.47	1	0.036	0.027	0.095	1.273	0.629
S_0	3.74	0.12	100.94	4.11	100.94	5	0.115	0.041	0.949	3.205	1.149
$S_{0.01}$	3.83	0.22	100.63	8.94	109.11	1	0.033	0.029	0.045	1.340	0.380
$S_{0.05}$	3.76	0.07	101.24	4.13	102.96	4	0.079	0.039	0.774	2.704	1.332

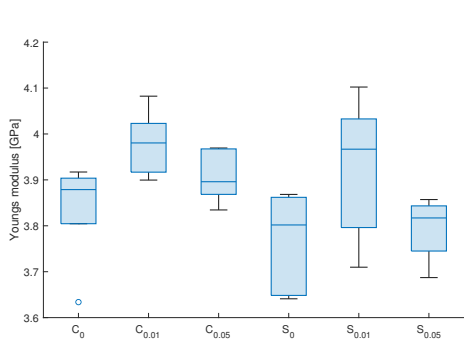

(a) Youngs' modulus [GPa]

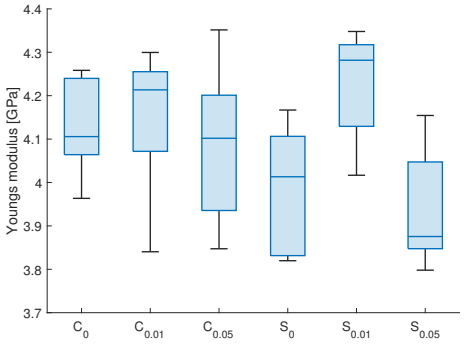

(b) Yieldstrength results σ_{max} [MPa]

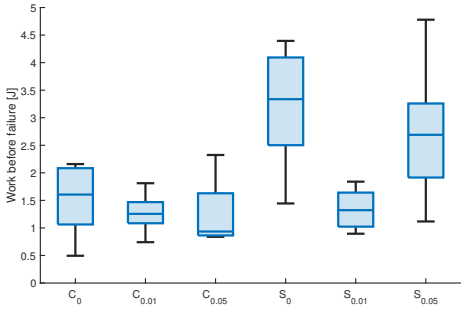

(c) Fracture toughness [J]

Figure 4.12: Results of mechanical testing

4.4.1 Discussion

In mechanical testing, the samples that were produced showed both very ductile and brittle responses. Contrary to the hypothesis no correlation between the GNP content and the ductility of the material was obvious. Some of the results show that at least the finely sieved polymer is capable of having a ductile response with strain at break values of 12 to 20 %. This level of ductility is reported in multiple sources [15, 56, 59, 43] in literature. The addition of GNP

and changing the crystal morphology was aimed at increasing the ductility, not decreasing it. Therefore a reason for the loss of ductility and transition to a brittle response must be isolated. For this transition either the entire material needs to be changed or this response can occur from local defects that fail before the rest of the material, increasing the overall stress and leading to complete failure. Three main point defects may have occurred in the material.

Origins of a brittle response

First, literature results showed that the addition of GNP to the polymer matrix leads to early and brittle fracture in many cases. This effect is generally attributed to stress localisation around clusters of GNP. A stack of GNP plates can work as a stress raiser since the GNP can have a very weak slip system, loading the material around it and causing the local stress raiser.
Due to thermal degradation the PEKK polymer can change chemically and deteriorate. Under an oxygen atmosphere near 400 °C PEKK has two main known degradation mechanisms, cross-linking and chain scission[15]. The first mechanism increases the effective molecular weight and the other decreases it. Over time the cross-linking mechanism is more active near 400 °C which causes a net increase in molecular weight leading to an increase of the T_g. Also, it has been reported that the melting enthalpy under the same processing conditions will decreases as the cross-linking mechanism stiffens the polymer chain and hinders crystallisation. These two effects cannot be seen in the DSC testing that was performed on the dogbone specimens. Indicating that these effects did not occur on a large scale in the material. There is however the possibility that local regions were degraded and created a weak point on which the specimens failed.
The third mechanism is the existence of voids in the dogbone specimens. Through compression mould there exists a risk that not all air was pushed out of the sample leaving small air pockets that carry no load and thus create stress concentrations around them. In only one sample a visible void was found on the fracture surface, which was in a C_0 sample. The Grade C powder, due to the large particle size did not pack down finely and could have trapped more air inside than the sieved powder fraction. The sieved powder also was noticeably more solid after pre-processing and packed down nicely while in powder form, possibly already eliminating most of the air that was trapped.
Comparing these mechanisms to the results leads to void formation during production as the most likely cause for the brittle response. Mainly because the brittle response is seen in all the samples produced from Grade C, which contains the larger polymer aggregates. The brittle break was even observed in the samples that contained no GNP and the thermal properties of the materials were virtually identical at the end of the production steps compared to the powders.

4.4.2 Fracture surfaces

The tensile testing results show the performance of the material. But to investigate the failure modes of the samples the fracture surfaces were investigated first by optical microscopy and then using SEM. Optical microscopy revealed the locations of failure initiation. Virtually all samples that showed little yielding in the tensile testing had an obvious failure point in the centreline of the width direction. A fracture surface of a brittly failed sample is shown in figure 4.13. This is an image taken using optical microscopy that shows the location of the defect but little about it's origin can be determined. Using SEM much more detail can be captured. Two micrographs are shown that indicate the general method of failure. Figure 4.14 shows the typical fracture surface that was found on the coarse powder blends. The surface is very jagged and shows small islands that look like flakes which indicate local crazing. Otherwise, the crack propagated at

such a speed that little is visible of the local microstructure.

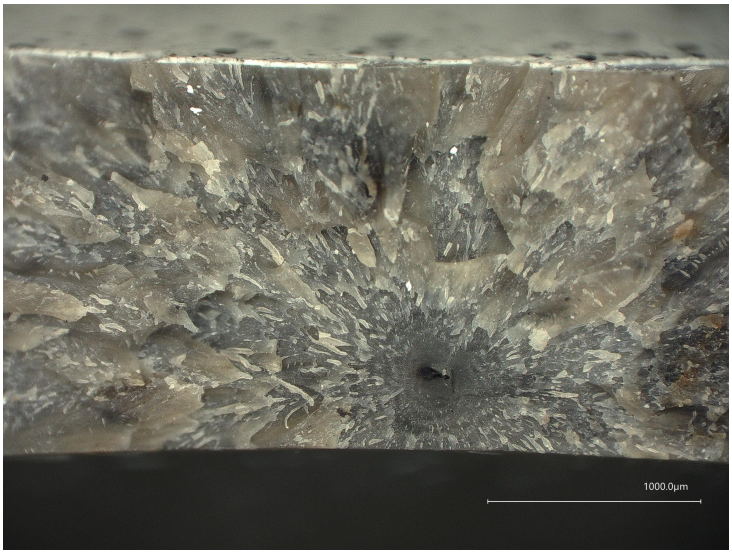

Figure 4.13: Optical microscopy image of fracture surface of a brittle failure in $C_{0.05}$

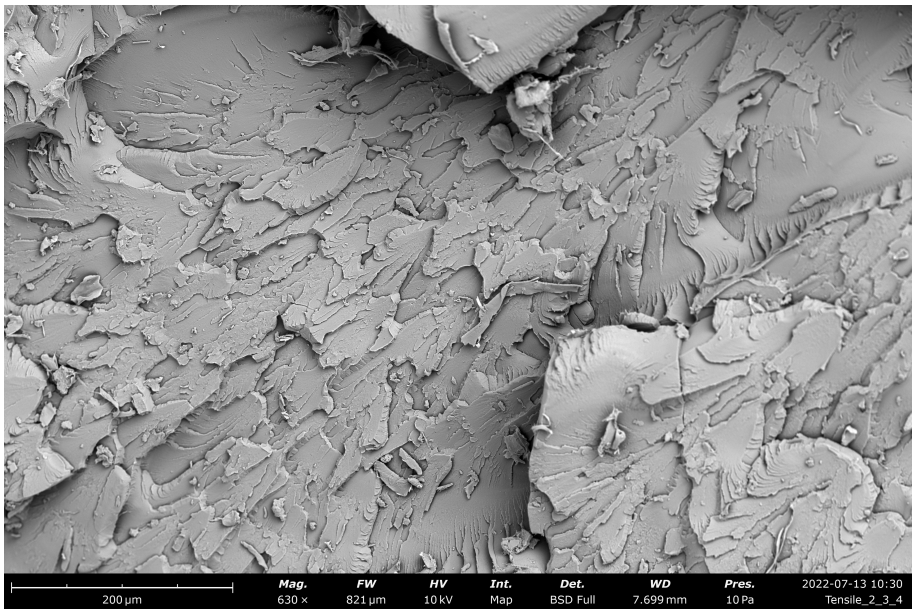

Figure 4.14: SEM image of the fracture surface of brittle break in specimen 2A ($C_{0.01}$)

Ductile failure shows a different fracture surface, one that is characterised by small fibrils which are typical for a necked and ductile failure of a polymer. In this fracture, much more new surface is created than in brittle fractures. Typically the outer corners of the specimen contain an area with local fibrillation as visible in figure 4.15. Then after a quarter width of the sample, there is a transition to beach marks [24] indicating a crack growth zone. More to the centre of the sample the microstructure is dominated by tall elongated structures that were formed during the necking and eventual fracture of the material. The transition to this zone is depicted in figure 4.16.

Another significant difference that was visible in the fracture surfaces of the $S_{0.05}$ samples presented in figure 4.16, is the presence of small features on the scale of the spherulite size found in the HSM analysis. These small structures also show shearlipping which is most likely from the inter spherulitic boundary that is plastically deforming under shear.

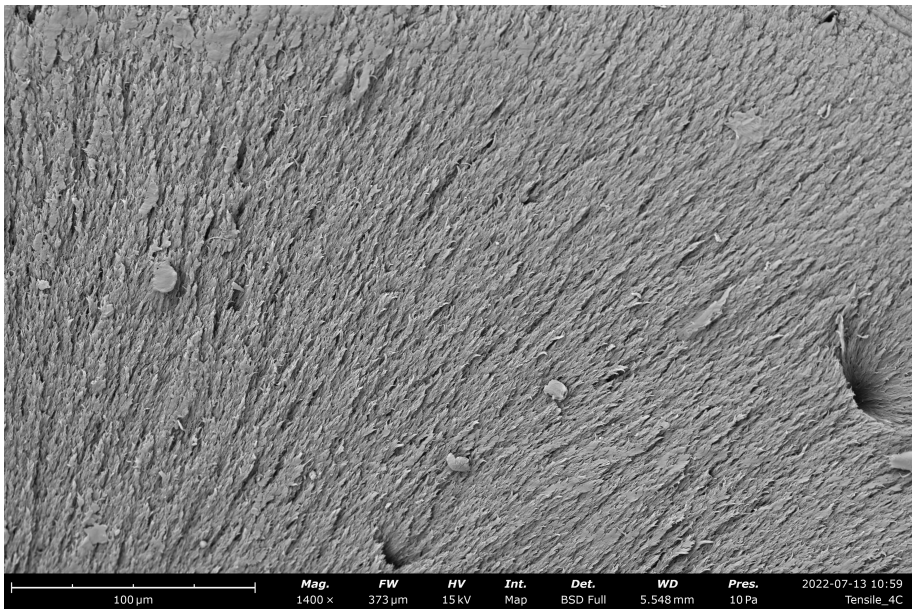

Figure 4.15: SEM image of the fracture surface of ductile break in specimen 4C ($S_{0.05}$)

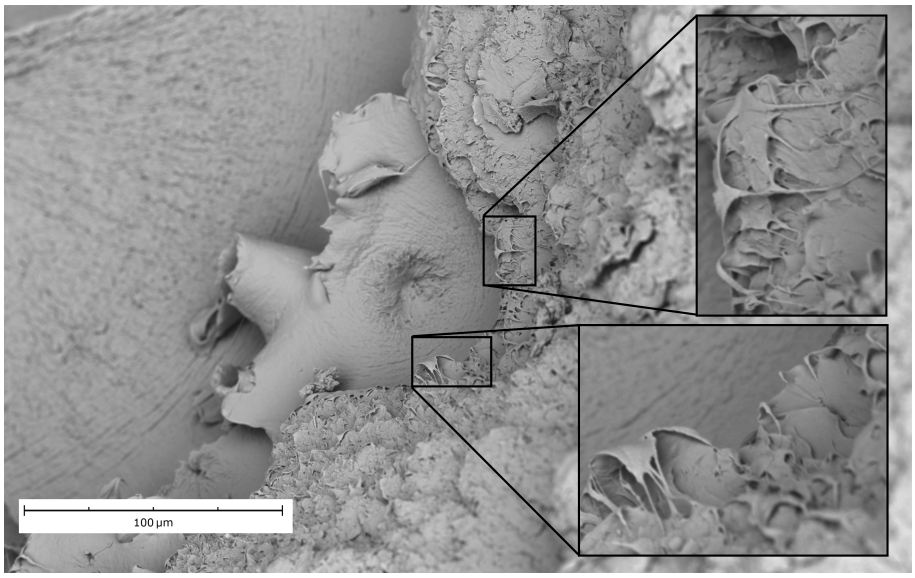

Figure 4.16: SEM image with details showing the fracture surface of ductile break in a ($S_{0.05}$) with the break moving from the top left to the bottom right.

4.5 Discussion

The effect of polymer crystal sizing has been an active area of study. Typically the microstructure was altered by controlling the cooling conditions. At high cooling rates ¿ 600 °C/min a poly aryl polymer cannot establish its crystalline structure resulting in amorphous material with high ductility but low stiffness [22], as the crystallinity of the material is also significantly lowered. Slow cooling rates around 1 to 5 °C/min produce fully crystallised samples with large spherulites with high stiffness but lower ductility [23, 15].

These changes to the crystal size were accompanied by a change in the relative crystallinity of the material. In the case of this research, the crystal size was changed while the relative crystallinity was still at a high or fully crystallised level. In general but also in polyaryl polymers the crystal formation of the spherulite is a region of very high crystallinity but the boundary between these spherulites presents a more amorphous character [35, 46, 54]. While the spherulites are stiffer than the amorphous boundary they are also more prone to crazing and cavitation which can lead to brittle behaviour [54].

The observation of an increase in the Youngs' modulus of the samples is consistent with observations by Schultz et al. [46]. Schultz combined many findings of the effect of spherulite size on mechanical properties. In a semi-crystalline polymer, there exists a discontinuity of elastic properties between the spherulites and the surrounding amorphous material. If we assume the amorphous boundary material to be less stiff than the spherulite itself, which is in accordance with findings [35]. Then under a general tensile load of the material the spherulite size changes the local material loading. As was first formulated by Schultz et al. and later found for PLA and PEO blends by Li et al. [32]. A larger spherulite will also create a larger strain in the inter lamellar layer proportional to the diameter.

In research from Choupin et al. [15] the same grade of Arkema kepstan 7002 was used and an interesting effect was noted on the mechanical properties of samples crystallised at low temperatures. *"Higher young's modulus and stress at yield have been observed for low crystallisation temperatures involving small spherulites which were attributed to a more homogeneous crystalline structure compared to large spherulites."* Here it is not only stated that a smaller spherulitic size is the path to better mechanical performance but homogeneity in the spherulitic size is essential. Therefore, the poor mechanical results of the $C_{0.01}$ and $C_{0.05}$ samples can be attributed to the few large spherulites that remain in the material. During deformation these can cause very high local strains in the inter-lamellar material causing a local premature failure. This void can then in turn cause the rest of the bulk material to fail.

5 CONCLUSIONS

This piece of research aims to answer the question *"What is the effect of changing the crystal morphology of poly ether ketone ketone through nucleating with graphene nanoplatelets on the mechanical properties of PEKK?"*. To answer this main question the PEKK polymer was evaluated using hot stage microscopy to evaluate the nucleation field, the results of which were confirmed by DSC testing. Also, the effects of shear flow on the distribution were taken into account and the mechanical properties of the polymer were evaluated using tensile testing.

How can the nucleation field homogeneity be evaluated and improved? With the large-scale hot stage experiments in combination with the crystal size estimation the nucleation field homogeneity could be evaluated. A large number of nuclei analysed meant enough data was available to analyse the outliers which comprise the inhomogeneities. Crystallisation peak width in DSC testing shows good congruence with the crystal size distribution and outliers from the HSM analysis.

What is the effect of the mixing method on the PEKK crystal morphology? The two alternative methods employed to improve the homogeneity of the crystallisation field showed to be effective at decreasing the areas with a low nucleation density. The use of small polymer particles works in the context of the research but is not as practical for industrial applications. Melt mixing worked as well and has a lower threshold to implementation as shear mixing is used abundantly in extrusion and compounding processes.

What is the influence of the PEKK crystal size and distribution on its mechanical properties? The mechanical properties of the PEKK samples were only marginally improved if at all. In tensile testing stress localisation happens before major deformation can occur in most samples. Work before failure was however not decreased in the sieved samples that contained 0.05%wt GNP, showing an improvement over literature results.

6 RECOMMENDATIONS

During this research, many interesting questions and suggestions for further research were compiled and are presented hereafter.

- For creating a PEKK polymer that is laced with a small amount of GNP it would be highly recommended to apply melt mixing. Preferably in the form of a high-shear mixer or an extruder. Using such a mixing process will circumvent all the variability in mixing that arises from the polymer particle size.
- Further testing on PEKK with a small spherulitic size needs to be conducted in impact testing or preferably by in-situ observation of the crystal structure during deformation. Such as on an SEM with an in-situ tensile tester.
- To improve the HSM results and make them more suitable for determining N0. A very thin film of around 5 µm could be used or the glass slides could be produced using vacuum forming.
- To allow more liberal characterisation of the PEKK polymer with finer crystallinity microstructure could also be created by self-seeding or isothermal crystallisation at lower temperatures. This would circumvent the need to preprocess the material and thus reduce the influence of earlier processing steps.
- DSC showed different crystallisation behaviour for the two pure grades of PEKK in film form. Using HSM to observe the films when melting it could be determined if these films have a typical spherulitic structure or an elongated crystal form.

Bibliography

[1] Arkema. Technical data – 7000 series product description. Technical report, Arkema, 2012.

[2] T.E. Attwood, P.C. Dawson, J.L. Freeman, L.R.J. Hoy, J.B. Rose, and P.A. Staniland. Synthesis and properties of polyaryletherketones. *Polymer*, 22(8):1096–1103, 1981.

[3] Eug. Bamberger and Fred Tschirner. Ueber die einwirkung von diazomethan auf arylhydroxylamine. *Berichte der deutschen chemischen Gesellschaft*, 33(1):955–959, 1900.

[4] John Bishopp. Adhesives for aerospace structures. In *Handbook of Adhesives and Surface Preparation*, pages 301–344. Elsevier, 2011.

[5] R. M. Blinstrub. xgnp® graphene nanoplatelets - grade c. Technical report, June 2021.

[6] BloombergNEF. Jet fuel demand gets a thrashing until 2026. *Bloomberg*, November 2020.

[7] D.J. Blundell and B.N. Osborn. The morphology of poly(aryl-ether-ether-ketone). *Polymer*, 24(8):953–958, 8 1983.

[8] Jr Willard Hallam Bonner. Aromatic polyketones and preparation thereof, 1959.

[9] F.A. Bovey. MACROMOLECULES IN THE SOLID STATE: MORPHOLOGY. In *Macromolecules*, pages 317–337. Elsevier, 1979.

[10] I.Y. Chang and J.K. Lees. Recent development in thermoplastic composites: A review of matrix systems and processing methods. *Journal of Thermoplastic Composite Materials*, 1(3):277–296, 7 1988.

[11] Saber Ayoub Chelaghma, Olivier De Almeida, Philippe Margueres, Jean-Charles Passieux, Jean-Noël Perie, Alain Vinet, and Bénédicte Reine. Identification of isothermal crystallization kinetics of poly(ether-ketone-ketone) based on spherulite growth measurements and enthalpic data. *POLYMER CRYSTALLIZATION*, 3(4), 8 2020.

[12] Binling Chen, Silvia Berretta, Ken Evans, Kaylie Smith, and Oana Ghita. A primary study into graphene/polyether ether ketone (PEEK) nanocomposite for laser sintering. *Applied Surface Science*, 428:1018–1028, January 2018.

[13] Eric J. H. Chen and Benjamin S. Hsiao. The effects of transcrystalline interphase in advanced polymer composites. *Polymer Engineering and Science*, 32(4):280–286, 2 1992.

[14] Kilwon Cho, Dohwan Kim, and Soong Yoon. Effect of substrate surface energy on transcrystalline growth and its effect on interfacial adhesion of semicrystalline polymers. *Macromolecules*, 36(20):7652–7660, 9 2003.

[15] Tanguy Choupin. *Mechanical performances of PEKK thermoplastic composites linked to their processing parameters*. Theses, Ecole nationale supérieure d'arts et métiers - ENSAM, 12 2017.

[16] Liangyong Chu, Wouter J. B. Grouve, Martin Drongelen, Erik G. Vries, Remko Akkerman, and Matthijn B. Rooij. Formation of flat-on lamellar crystals in absence of nanoconfinement. *Advanced Materials Interfaces*, 8(7):2001894, 2 2021.

[17] Liangyong Chu, Wouter J. B. Grouve, Martin van Drongelen, Yash Guha, Erik G. de Vries, Remko Akkerman, and Matthijn B. de Rooij. Influence of the polymer interphase structure on the interaction between metal and semicrystalline thermoplastics. *Advanced Engineering Materials*, 23(2):2000518, oct 2020.

[18] Luis Quiroga Cortés, Nicolas Caussé, Eric Dantras, Antoine Lonjon, and Colette Lacabanne. Morphology and dynamical mechanical properties of poly ether ketone ketone (PEKK) with meta phenyl links. *Journal of Applied Polymer Science*, 133(19):n/a–n/a, 2 2016.

[19] Abhinav Doddahanumegowda. Improving the ti/pekk joint performance by tuning the interphase crystalline structure using graphite nano-plates. Master's thesis, University of Twente, 2021.

[20] S.C. Freilich and F.S. Ohuchi. Reactions at the polyimide-metal interface. *Polymer*, 28(11):1908–1914, 10 1987.

[21] D. Galpaya, M. Wang, G. George, N. Motta, E. Waclawik, and C. Yan. Preparation of graphene oxide/epoxy nanocomposites with significantly improved mechanical properties. *Journal of Applied Physics*, 116(5):053518, August 2014.

[22] Shang-Lin Gao and Jang-Kyo Kim. Cooling rate influences in carbon fibre/PEEK composites. part 1. crystallinity and interface adhesion. *Composites Part A: Applied Science and Manufacturing*, 31(6):517–530, 6 2000.

[23] K. C. H Gardner, B. S. Hsiao, R. R. Matheson, and B. A. Wood. Structure, crystallization and morphology of poly (aryl ether ketone ketone). *Polymer*, 33(12):2483–2495, 1 1992.

[24] Jorge Luis González-Velázquez. Fractographyand failureanalysis, 2018.

[25] László Gránásy, Tamás Pusztai, György Tegze, James A. Warren, and Jack F. Douglas. Growth and form of spherulites. *Physical Review E*, 72(1):011605, July 2005.

[26] Brandon Graver, Dan Rutherford, and Sola Zheng. Co2 emissions from commercial aviation: 2013, 2018, and 2019. resreport, The international council on clean transportation, October 2020.

[27] Max Roser Hannah Ritchie and Pablo Rosado. Energy. *Our World in Data*, 2020. https://ourworldindata.org/energy.

[28] Yenny Hernandez, Valeria Nicolosi, Mustafa Lotya, Fiona M. Blighe, Zhenyu Sun, Sukanta De, I. T. McGovern, Brendan Holland, Michele Byrne, Yurii K. Gun'Ko, John J. Boland, Peter Niraj, Georg Duesberg, Satheesh Krishnamurthy, Robbie Goodhue, John Hutchison, Vittorio Scardaci, Andrea C. Ferrari, and Jonathan N. Coleman. High-yield production of graphene by liquid-phase exfoliation of graphite. *Nature Nanotechnology*, 3(9):563–568, 8 2008.

[29] ISO. Plastics - test specimens. Standard, Geneva, CH, December 2018.

[30] Emmanuelle Koscher and René Fulchiron. Influence of shear on polypropylene crystallization: morphology development and kinetics. *Polymer*, 43(25):6931–6942, 1 2002.

[31] Andrey E. Krauklis, Christian W. Karl, Abedin I. Gagani, and Jens K. Jørgensen. Composite material recycling technology—state-of-the-art and sustainable development for the 2020s. *Journal of Composites Science*, 5(1):28, 1 2021.

[32] Jin-Ze Li, Jerold M. Schultz, and Chi-Ming Chan. The relationship between morphology and impact toughness of poly(l-lactic acid)/poly(ethylene oxide) blends. *Polymer*, 63:179–188, April 2015.

[33] Vanessa M. Marinosci, Wouter J.B. Grouve, Matthjn B. de Rooij, Sebastiaan Wijskamp, and Remko Akkerman. Effect of grit-blasting on the fracture toughness of hybrid titanium-thermoplastic composite joints. *International Journal of Adhesion and Adhesives*, 109:102893, 9 2021.

[34] V.M. Marinosci, L. Chu, W.J.B. Grouve, S. Wijskamp, R. Akkerman, and M.B. de Rooij. Characterization of the water–titanium interaction and its effect on the adhesion of titanium-c/PEKK joints. *Composites Part A: Applied Science and Manufacturing*, 162:107107, November 2022.

[35] V.M. Marinosci, N.G.J. Helthuis, L. Chu, W.J.B. Grouve, M.B. de Rooij, S. Wijskamp, and R. Akkerman. The role of process induced polymer morphology on the fracture toughness of titanium–PEKK interfaces. *Engineering Fracture Mechanics*, 268:108475, 6 2022.

[36] Mohammad Mehrali, Emad Sadeghinezhad, Sara Tahan Latibari, Salim Newaz Kazi, Mehdi Mehrali, Mohd Nashrul Bin Mohd Zubir, and Hendrik Simon Cornelis Metselaar. Investigation of thermal conductivity and rheological properties of nanofluids containing graphene nanoplatelets. *Nanoscale Research Letters*, 9(1), 1 2014.

[37] Peter Merlin. Design and development of the blackbird: Challenges and lessons learned. In *47th AIAA Aerospace Sciences Meeting including The New Horizons Forum and Aerospace Exposition*. American Institute of Aeronautics and Astronautics, 1 2009.

[38] A. Mouritz. *Introduction to aerospace materials.pdf*. WOODHEAD PUB, June 2012.

[39] Géraldine Oliveux, Luke O. Dandy, and Gary A. Leeke. Current status of recycling of fibre reinforced polymers: Review of technologies, reuse and resulting properties. *Progress in Materials Science*, 72:61–99, July 2015.

[40] Lingling Ou, Bin Song, Huimin Liang, Jia Liu, Xiaoli Feng, Bin Deng, Ting Sun, and Longquan Shao. Toxicity of graphene-family nanoparticles: a general review of the origins and mechanisms. *Particle and Fibre Toxicology*, 13(1), October 2016.

[41] Helena Pérez-Martín, Paul Mackenzie, Alex Baidak, Conchúr M. Ó Brádaigh, and Dipa Ray. Crystallinity studies of PEKK and carbon fibre/PEKK composites: A review. *Composites Part B: Engineering*, 223:109127, 2021.

[42] S.J. Pickering. Recycling technologies for thermoset composite materials—current status. *Composites Part A: Applied Science and Manufacturing*, 37(8):1206–1215, August 2006.

[43] J.A. Puértolas, M. Castro, J.A. Morris, R. Ríos, and A. Ansón-Casaos. Tribological and mechanical properties of graphene nanoplatelet/PEEK composites. *Carbon*, 141:107–122, 1 2019.

[44] W. G. Roeseler, B. Sarh, and M. U. Kismarton. Composite structures: The first 100 years. In *ICCM International Conferences on Composite Materials*, 2007.

[45] T. Sadowski, M. Kneć, and P. Golewski. Experimental investigations and numerical modelling of steel adhesive joints reinforced by rivets. *International Journal of Adhesion and Adhesives*, 30(5):338–346, 7 2010.

[46] J. M. Schultz. Microstructural aspects of failure in semicrystalline polymers. *Polymer Engineering and Science*, 24(10):770–785, July 1984.

[47] Andreas Schwitalla and Wolf-Dieter Müller. PEEK dental implants: A review of the literature. *Journal of Oral Implantology*, 39(6):743–749, dec 2013.

[48] Ge Shi, Sherif Araby, Christopher T. Gibson, Qingshi Meng, Shenmin Zhu, and Jun Ma. Graphene platelets and their polymer composites: Fabrication, structure, properties, and applications. *Advanced Functional Materials*, 28(19):1706705, 3 2018.

[49] Chih-Jen Shih, Shangchao Lin, Michael S. Strano, and Daniel Blankschtein. Understanding the stabilization of liquid-phase-exfoliated graphene in polar solvents: Molecular dynamics simulations and kinetic theory of colloid aggregation. *Journal of the American Chemical Society*, 132(41):14638–14648, 10 2010.

[50] Sasha Stankovich, Dmitriy A. Dikin, Geoffrey H. B. Dommett, Kevin M. Kohlhaas, Eric J. Zimney, Eric A. Stach, Richard D. Piner, SonBinh T. Nguyen, and Rodney S. Ruoff. Graphene-based composite materials. *Nature*, 442(7100):282–286, July 2006.

[51] Y. Su. *Co-consolidation of titanium-C/PAEK joints: an investigation into the interfacial performance governing mechanisms*. PhD thesis, University of Twente, January 2017.

[52] Yibo Su, Matthijn de Rooij, Wouter Grouve, and Remko Akkerman. The effect of titanium surface treatment on the interfacial strength of titanium – thermoplastic composite joints. *International Journal of Adhesion and Adhesives*, 72:98–108, January 2017.

[53] John Texter. Graphene dispersions. *Current Opinion in Colloid & Interface Science*, 19(2):163–174, 4 2014.

[54] C. Thomas, R. Seguela, F. Detrez, V. Miri, and C. Vanmansart. Plastic deformation of spherulitic semi-crystalline polymers: An in situ AFM study of polybutene under tensile drawing. *Polymer*, 50(15):3714–3723, July 2009.

[55] Fuzhong Wang, Lawrence T. Drzal, Yan Qin, and Zhixiong Huang. Enhancement of fracture toughness, mechanical and thermal properties of rubber/epoxy composites by incorporation of graphene nanoplatelets. *Composites Part A: Applied Science and Manufacturing*, 87:10–22, aug 2016.

[56] Q. B. Wang, D. L. Jia, X. H. Pei, X. L. Wu, F. Xu, Z. H. Ye, and H. X. Wang. Mechanical performance of graphenex/poly(ether ketone ketone) composite sheets by hot pressing. *Scientific Reports*, 12(1), March 2022.

[57] Yuan Wang, Davood Rouholamin, Richard Davies, and Oana R. Ghita. Powder characteristics, microstructure and properties of graphite platelet reinforced poly ether ether ketone composites in high temperature laser sintering (HT-LS). *Materials & Design*, 88:1310–1320, December 2015.

[58] J. Wei, M.S. Saharudin, and T. Vo. N,n-dimethylformamide (DMF) usage in epoxy/graphene nanocomposites: Problems associated with reaggregation. *Polymers*, 9(12):193, 5 2017.

[59] Da Xu, Yanwei Gao, Yang Sun, Zhaoyang Wang, Zhenhua Jiang, Xiangyu Jiang, and Haibo Zhang. A novel graphene nanoplatelets (GNPs) dispersant: Polyaryletherketones with pendent pyrene groups. *Macromolecular Chemistry and Physics*, 220(9):1800553, 4 2019.

Appendix A Strain to displacement signal alignment

A distinct disadvantage of using the aramis setup is data collection is split over two computers with two different internal clocks. The Aramis recording needs to be started manually so there always is an unknown delay between the signals. Adding the task of aligning the signals in time during preprocessing of the data. An advantage of the large amount of data that the aramis setup provides is that some facets very near the clamps of the tensile tester are also recorded. These points show low strains and are not of interest as they are outside of the gauge length. But with these points the x-y-z coordinates of the clamps are also recorded. Using these points located at either end of the sample the elongation over the whole sample can be calculated which should be the same as the elongation signal from the Zwick/Roell machine.

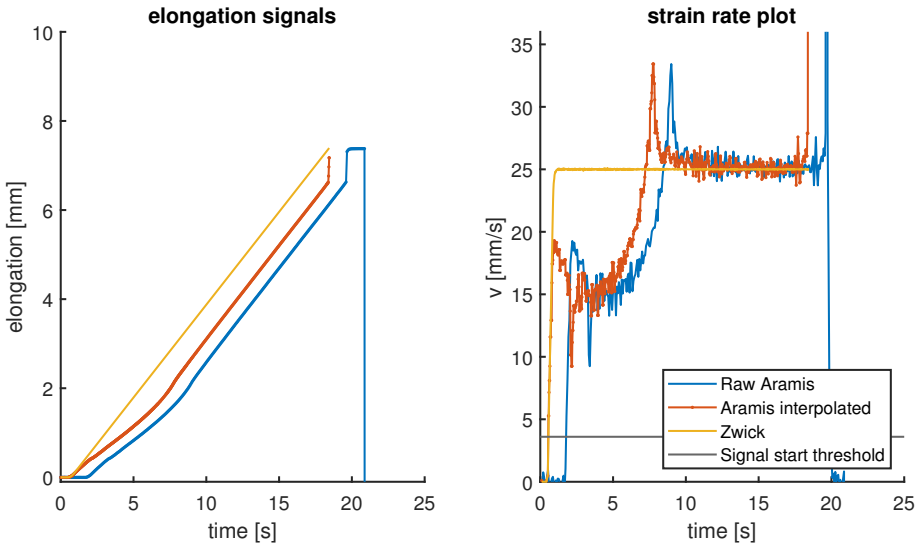

Figure A.1: Combined signals from Aramis and Zwick logs

The elongation signals can be seen in the left subfigure A.1. In the right subfigure the test speed is calculated by taking the forward difference of the elongation signals. These plots revealed some opportunities but also raised some concerns. First the raw Aramis signal lags significantly behind the zwick signal in time. This was corrected by finding the point in both signals where the testing speed rose above 3.6 mm/s, then the time vector of the Aramis signal was shifted such that these points line up.
In the elongation signal it is visible that the Aramis signal does not only lag behind in time but also in magnitude. In these few data points the signal rises the same as the Zwick signal. Then the test speed seen in the Aramis field is lower than the tensile tester is reporting. This effect is attributed to the settling of the comparatively heavy duty wedge grips. After 4 mm of travel the elongation signal become parallel again and the test speeds are exactly the same, but there is an offset of about 0.6 mm. After fracture of the sample and thus when the load on the grips has dissipated the elongation reported by the Zwick and Aramis setup line up again. This situation is not ideal and could have been mitigated if a smaller tensile tester was used but due to the extra data measured with the Aramis setup the problem is of no influence on the results.

Appendix B Full mechanical testing results

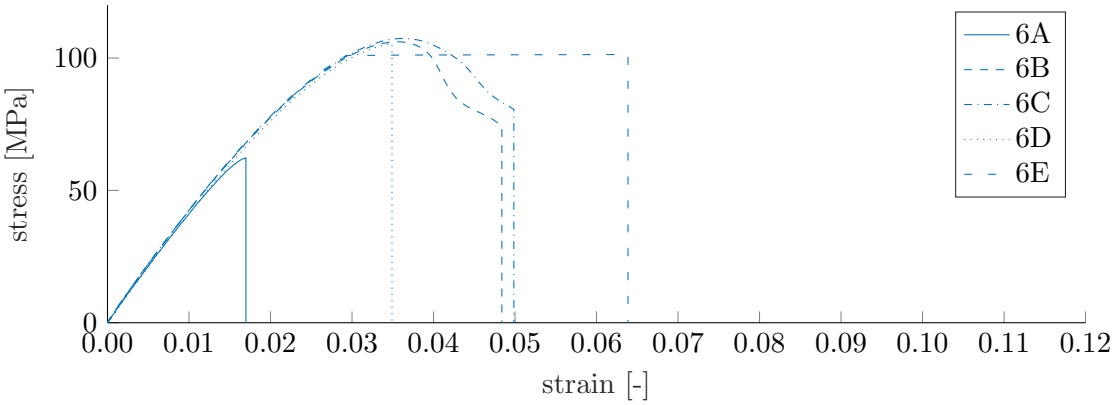

Figure B.1: C_0

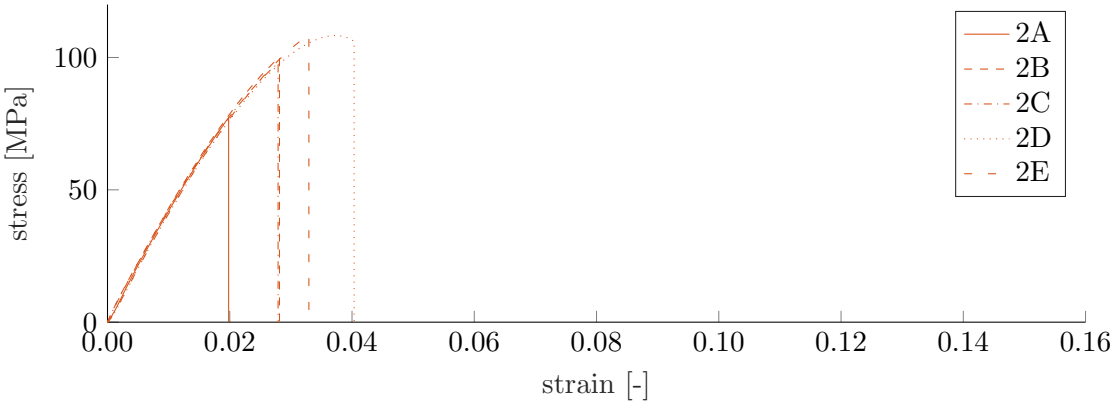

Figure B.2: $C_{0.01}$

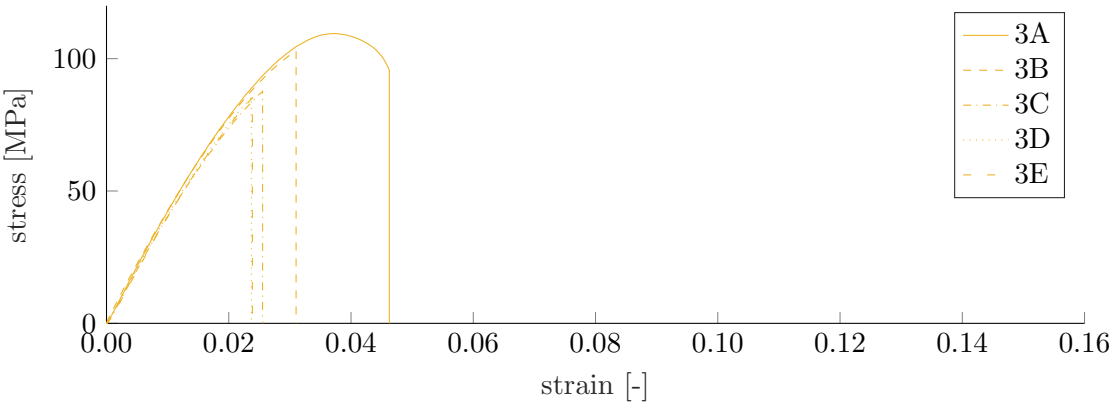

Figure B.3: $C_{0.05}$

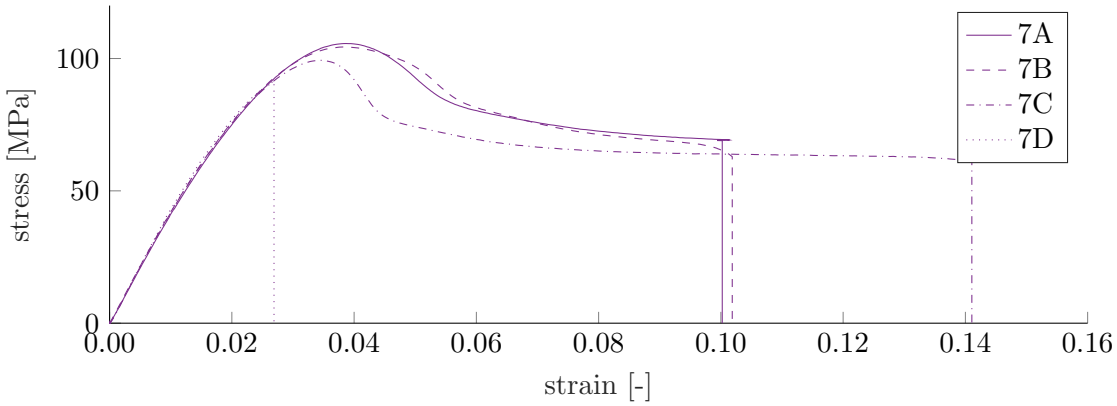

Figure B.4: S_0

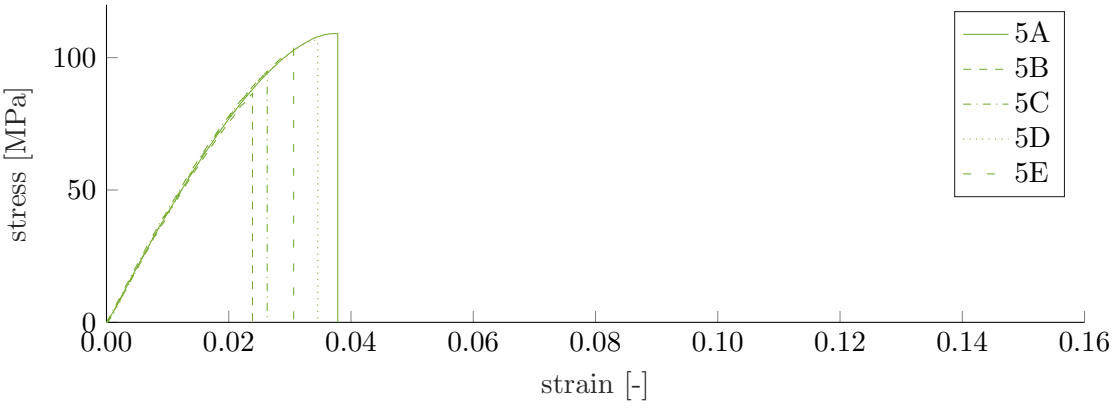

Figure B.5: $S_{0.01}$

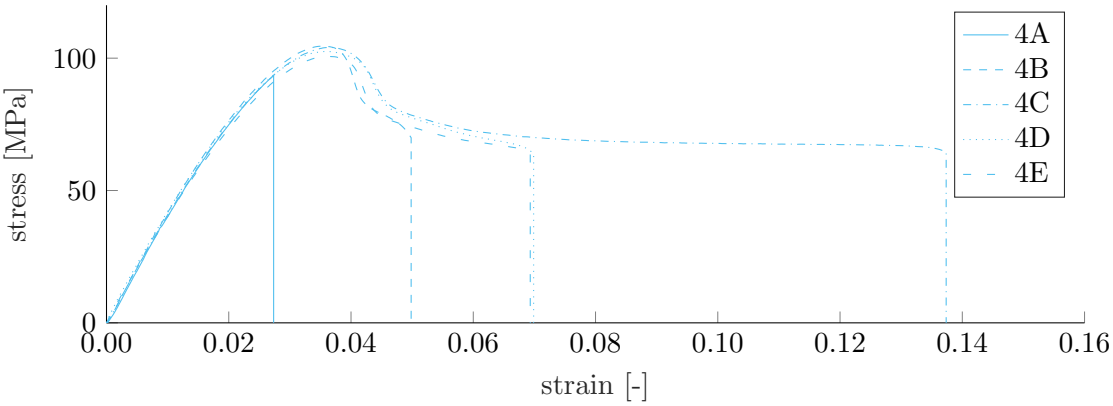

Figure B.6: $S_{0.05}$